Design, Fabrication and Evaluation of multiple Microfluidic model devices for enrichment of Circulating Tumour Cells from whole blood

Report on the results of *in vitro* capturing of human breast cancer cells using microfluidic devices

Simon de Regt

Wageningen University & Research

2017-2018

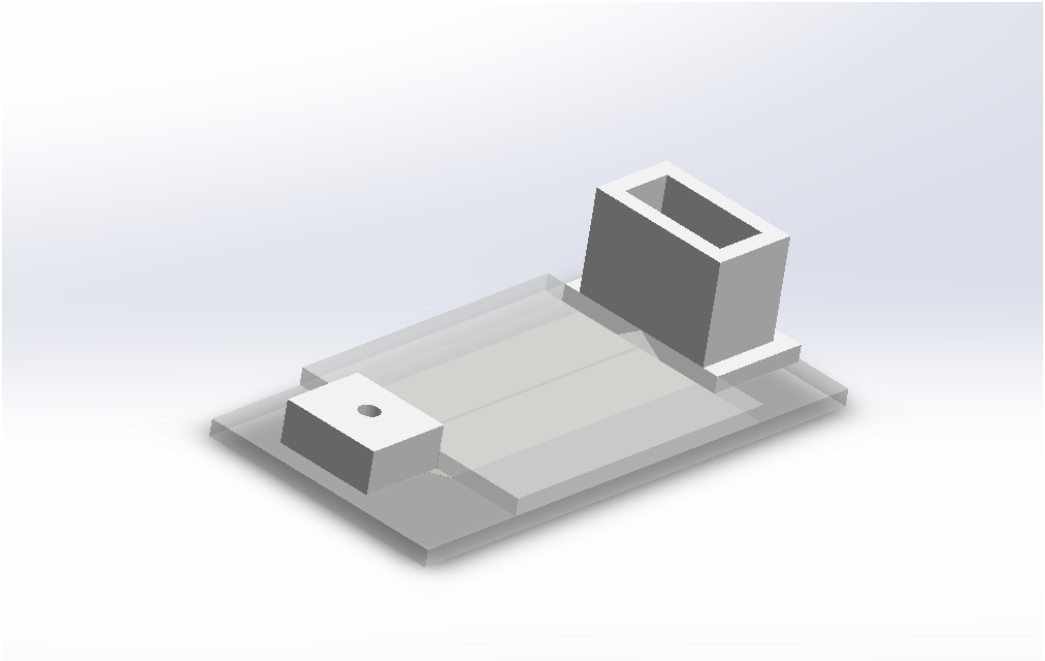

Title:	Design, Fabrication and Evaluation of multiple Microfluidic model devices for enrichment of Circulating Tumour Cells from whole blood
Author:	**S.L. (Simon) de Regt**, 941229683030
Supervisor:	**P. (Pepijn) Beekman** MSc Wageningen University & Research, University of Twente
1st Examiner:	Dr.ir. **M.M.J. (Maarten) Smulders** Wageningen University & Research
2nd Examiner:	Dr.ir. **A.T. (Albert) Poortinga** Technische Universiteit Eindhoven

Active Organic Surfaces group, Laboratory of Organic Chemistry, Wageningen University & Research. Chair holder: Prof.dr. **J.T. (Han) Zuilhof**

Wageningen, 10-2017 – 07-2018

Cover image: SolidWorks design of epoxy model device IV.

Preface

Imagine a river full of fish swimming with boats floating by. Here, the river simulates your blood flow, the algae are red blood cells, and the fish imitate blood cells such as lymphocytes and monocytes. As time goes by, billions of algae particles have travelled by, and you watched a million regular fish coming and going. You also noticed *one* odd fish for every million regular fish that passed by. Imagine it was a shark, which should not be swimming in this river! This shark represents a rare cancer cell that is the topic of interest in this thesis. On the outside it is clearly different from the regular fish, but the challenge is to catch this shark from the river without disturbing the other fish and algae.

I think the selective capturing of rare cells is a very elegant and powerful method for cell detection and enumerating in samples with low specific cell concertation. Having come across multiple fields of biotechnology, I found myself most interested in using and designing specialised analytical apparatus for research purposes. The idea of lab-on-chip and cytometric devices are in my opinion interesting and rewarding causes to put my full attention to.

Without the input of dr. Jacob Baggerman and the guidance of Pepijn Beekman this project would not have been possible. It was motivating to be a part of the team from Han Zuilhof, who has been appointed Fellow of Royal Society of Chemistry.

Abstract

Over 90% of all cancer-related deaths are not caused by the primary tumour, but from secondary tumours which form from cells that shed from the primary tumour. The shed cells can enter the blood stream and become Circulating Tumour Cells (CTCs). The CTC concentration is an indication for the disease prognosis. The challenge, however, is the limited number of CTCs that are present in blood (about 1-10 per millilitre). There is already an FDA-approved CTC-capturing method available (CellSearch®, Janssen Diagnostics, USA) but this method analyses a blood sample of only 7.5 mL, meaning it is often not possible to obtain sufficient CTCs to reach statistically significant clinical conclusions.

To solve the problem of capturing too few CTCs, multiple blood filtration devices that could be operated continuously (5 L in 24 h) while capturing CTCs were designed, fabricated, and evaluated based on their cell capture ability at different flow velocities, sample throughput, cell distribution in the channel, and cell recovery. Anti-epithelial cell adhesion molecule antibodies (anti-EpCAM) were immobilised onto polyacrylic acid (PAA) functionalised glass to specifically bind EpCAM antigens on the surface of MCF-7 human breast cancer cells to capture epithelial tumour cells without non-specific binding of blood cells.

Most importantly, cell capture occurred in the first 1 mm of the channel and enriching target cell from whole blood was successful. These results are proof-of-principle for a future microsieve device with 1 mm deep pores to capture MCF-7 cells from blood. By employing a channel height equal to the cell diameter (to force cells to interact with the antibody coating within the channels), we achieved two times higher linear flow velocity and 25 times higher flow rate per channel than previously reported for similar devices. These results allow large sample analysis in reasonable time and a decrease of non-specific binding of blood cells. Altering the pH or ionic strength proved to be promising methods to detach captured cells without rupturing their membrane, which is important for cell enumeration and downstream cell characterisation.

Our results demonstrate the feasibility of a continuously operated future microsieve. We anticipate that continuous sampling could be a valuable technology in clinical setting for detection of metastatic disease and monitoring therapy efficacy.

Keywords: metastatic disease, circulating tumour cells, CTC, microfluidics, affinity-based capturing, EpCAM

Contents

List of abbreviations

AO	acridine orange
BF	bright field
CTC	circulating tumour cell
DAPI	4′,6-diamidino-2-phenylindole
DMEM	Dulbecco's modified Eagle's medium
EDC	1-ethyl-3-(3-dimethyl-aminopropyl) carbodiimide
EDTA	ethylenediaminetetraacetic acid
EpCAM	epithelial cell-adhesion molecule
FBC	fetal bovine serum
HTMSU	high-throughput micro-sampling unit
ISET	Isolation by Size of Epithelial Tumour cells
Anti-IgG-PE	anti-immunoglobulin G-R-phycoerythrin
MCF-7	Michigan Cancer Foundation-7
MDA-MB-231	M.D. Anderson Cancer Center metastatic breast cancer-231
MES	2-(N-morpholino)ethanesulfonic acid
MQ	Milli-Q
NHS	N-Hydroxysuccinimide
ORC	laboratory of organic chemistry
PBS	phosphate-buffered saline
PDMS	polydimethylsiloxane
PET	polyethylene terephthalate
RBC	red blood cell
SD	standard deviation
TE	trypsin/EDTA solution
TR	Texas Red
UV	ultraviolet

Introduction

Problem definition: death rate in humans by metastatic cancer

Cancer is a disease characterised by the rapid multiplication of abnormal cells and tissue growth beyond its usual boundaries (Centre, 2017). 45.279 people died from cancer in The Netherlands in 2016, making it the leading cause of death (StatLine, 2017), see *Figure 1*. Globally, almost 1 in 6 deaths is due to cancer (Centre, 2017). 90% cancer-related deaths are not caused by the primary tumour itself, but from metastasis (Centre, 2017; Plaks, Koopman, & Werb, 2013). The primary tumour can accumulate mutations and become malignant and metastasize. In metastatic phase, the primary tumour sheds its cells or cell clumps into the peripheral blood stream or into the lymphatic system (Liotta, Kleinerman, & Saldel, 1976; Muschel, 2011). Via these bodily networks, the shed cells travel through all parts of the body, can settle at suitable sites and grow to form secondary tumours or become dormant (Schwab, 2011; Szmulewitz, Taylor, & Rinker-Schaffer, 2011). This process of translocation was already described in 1889 as ‘’seed and soil’’ hypothesis by Paget (Qian & Teh, 2011). Recently it was discovered that circulating tumour cells can adapt their metabolism to their new environment (‘’soil’’) (Bu et al., 2018). The cells that were shed from the primary tumour and circulate in the blood stream are called Circulating Tumour Cells (CTCs).

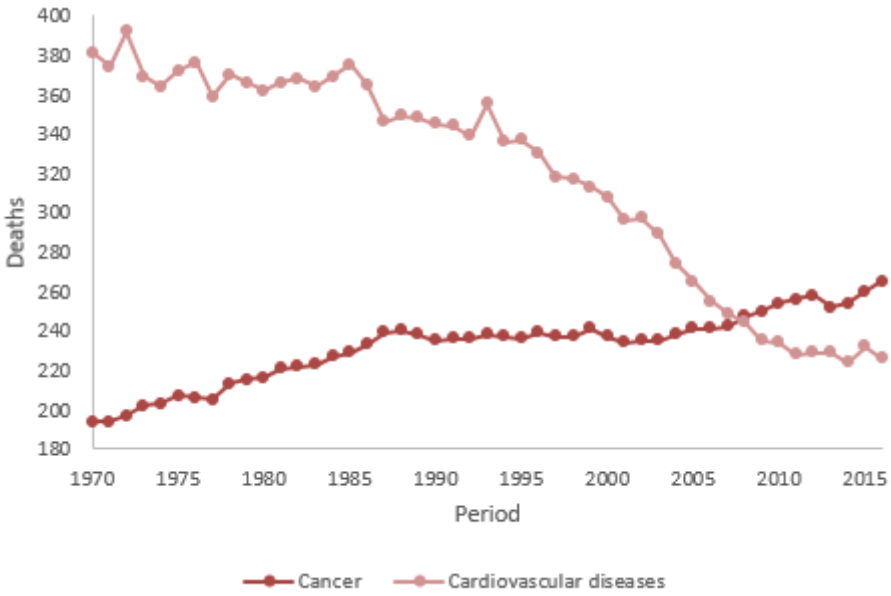

Figure 1 Number of death by malignant neoplasms (‘cancer’) and diseases of the circulatory system (‘cardiovascular diseases’) per 100 000 of the average population from 1970 to 2016. Data source: opendata.cbs.nl. (StatLine, 2018).

Clinical relevance of circulating tumour cells

Because of the high death rate of metastatic disease, clinical goals to reduce the mortality rate are focussed at (1) preventing formation of metastases (secondary tumours) and (2) designing effective therapies for patients with established metastatic disease (Stoecklein, Fischer, Niederacher, & Terstappen, 2016). Early diagnosis of metastatic disease is most important in managing goal (1), which could be achieved via early detection of the presence of CTCs. For goal (2), captured CTCs could be used to choose the appropriate and personalised clinical therapy and to judge the disease prognosis in real-time (Muschel, 2011). CTCs captured from blood via a minimally invasive liquid blood biopsy via a venipuncture and act as reliable biomarkers for early metastatic detection, prognosis prediction, appropriate therapy determination, primary tumour localisation, and real-time disease treatment monitoring (Plaks et al., 2013).

Prognosis prediction: The presence and concentration of CTCs correlates with increased patient mortality rates (F. A. Coumans, Ligthart, Uhr, & Terstappen, 2012; F. A. W. Coumans, Doggen, Attard, de Bono, & Terstappen, 2010; Cristofanilli et al., 2004; Danila et al., 2007; Moreno et al., 2005). Even for non-metastatic cancer patients (no secondary tumours are formed yet) the concentration of CTCs might provide prognostic information (Lucci et al., 2012).

Localisation of the primary tumour: Currently, the primary tumour could not be found in 3-9% of the cancer patients that are diagnosed with the presence of metastases (secondary tumours) (Moran et al., 2016). This inhibits site-specific therapy, resulting in poor prognosis. As it is possible with metastatic tumour samples (Moran et al., 2016), it might also be possible to use CTCs for localisation of the primary tumour by analysing the CTCs physiological and organ-specific genetic and epigenetic information.

Biological data: CTCs can provide plenty information on intra-tumour heterogeneity and tumour evolution, such as the mutation status of critical genes (Y. P. Hong & Zhang, 2016; Strati, Kasimir-Bauer, Markou, Parisi, & Lianidou, 2013) and the cellular pathways underlying tumour progression (F. A. Coumans et al., 2012). Also, as metastatic disease research is ongoing, biomedical research on metastasis general could benefit from CTC capturing data to better understand the process of metastasis (Nagrath et al., 2007).

The main challenge with circulating tumour cells

As outlined in the previous section, it becomes apparent that detecting cancer cells that are circulating in the body is of great relevance in clinical setting, but there is a challenge: CTCs are rare. Although a tumour can release millions of CTCs per day, the CTC can have a very low abundance number relative to the vast number of red blood cells and white blood cells (*Figure 2-A*) (Bockhorn, Jain, & Munn, 2007; Nagrath et al., 2007; Stoecklein et al., 2016). About 1-10 CTCs are found per millilitre blood, while this blood volume contains billions of peripheral mononuclear cells (PBMCs; monocytes and lymphocytes) and red blood cells (RBCs) (Adams et al., 2008; Ross et al., 1993; Sleijfer et al., 2007). CTCs are quite similar to blood cells regarding cell size and cell density (*Figure 2-B, C*), so simple methods like size-based filtration and centrifugation are not selective. Therefore, the technologies required for CTC detection therefore need to be sensitive and robust (Allan & Keeney, 2010; Schwab, 2011)

Even with sensitive and robust technology, it could occur that from a small sample volume zero CTCs are found in patients with metastatic disease, because there are simply too few CTCs present in the patient. In studies using the only FDA-approved technology for CTC enumeration CellSearch®, 20% to 50% of blood samples of patients with metastatic disease were found to have 0 CTCs in 7.5 mL of blood (F. A. Coumans et al., 2012). Moreover, CellSearch® detects over 3-fold *fewer* cells compared to flow cytometry (FC) using the same blood volume (F. A. Coumans et al., 2012). Flow cytometry is an expensive though extremely sensitive tool to detect cell surface and intracellular antigens by. It analyses all cells individually, hence this technology is a powerful comparative tool to determine cell loss in other assays.

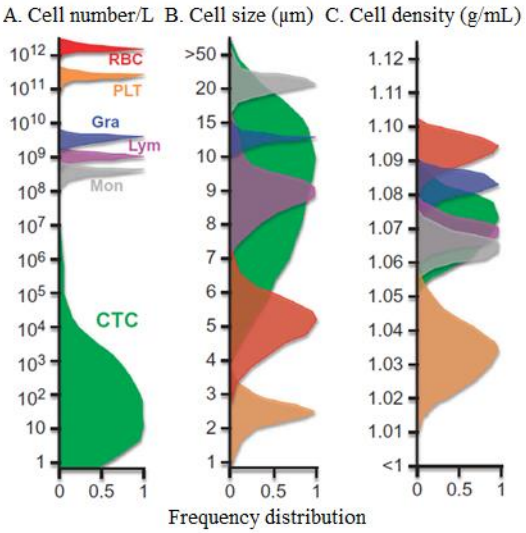

Figure 2 (A) Number of cells per litre blood, (B) cell size in micrometres, and (C) cell density in g.mL^{-1}. Blood cells: erythrocytes (RBC), platelets (PLT), granulocytes (Gra), lymphocytes (Lym), monocytes (Mon), and circulating tumour cells (CTC). Adapted from (Stoecklein et al., 2016).

The basis of the capturing method: antigens and antibodies

The goal of this thesis is improving CTC enumeration technology, so CTCs need to be enrichment from blood by capturing them. The basis of this capturing method is explained here.

There are four major tissue types: epithelial, connective, muscular and nerve tissue. Differences in surface characteristics of cells from different tissue types (tissue-type specific antigens) are used to separate CTCs from blood cells. Tumour cells can be captured specifically from a heterogeneous sample (blood) by antibodies that selectively bind with epithelial antigens, because blood cells (connective tissue) do not contain these epithelial antigens on their surface (*Figure 3*).

More specifically, the antigen of interest in this thesis is Epithelial Cell Adhesion Molecule (EpCAM, CD326), which is overexpressed in a multitude of tumours, e.g. colon, breast, prostate, head and neck, and liver but not expressed in non-epithelial cells (Macdonald et al., 2018; Sterzynska, Kempisty, Zawierucha, & Zabel, 2012). EpCAM is a transmembrane glycoprotein that is involved in cell-cell adhesion (Macdonald et al., 2018), cell signalling, migration, proliferation and differentiation (Ni et al., 2012). One cell type used in this thesis overexpresses this antigen (1), while the other cell type has decreased expression of this antigen (2):

(1) ***MCF-7***, EpCAM positive, adherent, human mammary gland, ~18µm in diameter;
(2) ***MDA-MB-231***, EpCAM negative (~50 times lower EpCAM expression compared with MCF-7, unpublished data), adherent, human mammary gland, ~18µm in diameter.

Specific 'anti-epithelial' antibodies (binding to epithelial antigens) were immobilised inside the channels of the microfluidic devices in this thesis. Henceforth referred to as anti-EpCAM antibodies.

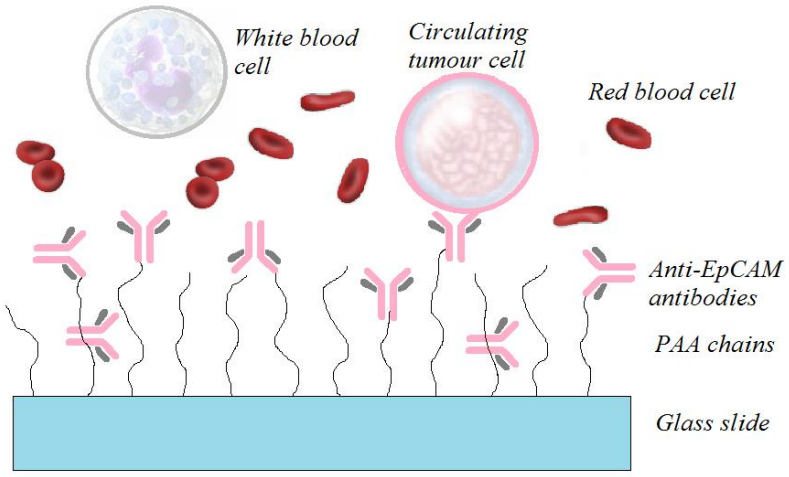

Figure 3 Schematic representation (not to scale) of the bottom glass slide with anti-EpCAM antibodies bound to poly-acrylic acid chains. The red blood cells and the white blood cell cannot bind with these antibodies, while the circulating tumour cell has specific antigens on its surface that bind with the anti-EpCAM antibodies. White blood cell and circulating tumour cell image adapted from www.cancer.gov/types/leukemia/patient/hairy-cell-treatment-pdq, retrieved 18-06-2018.

Microfluidic devices: benefits and limitations

This thesis used devices that are considered a microfluidic devices. Micro- and nanoscale technologies have certain benefits over regular-scale analytical technologies, such as flow cytometry. Compared to macro-scale technologies, micro-scale devices require less sample and reagent volume, allow fast sample processing, have high sensitivity, are sometimes cheaper, allow point-of-care diagnostics and thereby have a reduced clinical processing time, have improved sterility by cross-contamination prevention due to disposability and sometimes autoclave-ability, and have the potential to be integrated with other analytical technologies (Barteneva, Ketman, Fasler-Kan, Potashnikova, & Vorobjev, 2013; E. Ng, Hoshino, & Zhang, 2013; S. Y. Ng et al., 2010; Radisic, Iyer, & Murthy, 2006; Yusa et al., 2014; Zhang et al., 2016). The general limitations of microfluidic chips are their maximum processing volume and difficulty in fabrication.

In vivo microfluidic technology

Microfluidic devices have, because of the above mentioned benefits, the possibility to be placed *in vivo*, of which the GILUPI CellCollector™ (Gilupi Nanomedizin, *Figure 4*) is an example. This is an *in vivo* CTC isolation device comprising of an anti-EpCAM functionalised medical wire that is placed directly into the blood stream in the arm of the patient for 30 minutes (Saucedo-Zeni et al., 2012; Theil et al., 2016).

The downsides of this device are the over two-hour processing time required before cell enumeration is possible and cell recovery rates of only 10-35%. Cell recovery is the number of captured target cells relative to the total number of target cells that passed by. Two possible explanation for the low cell recovery: (1) not all cells encountered the wire while passing through the vein and/or (2) captured cells are detached during washing steps because of too low antigen-antibody bond strength.

As a solution to problem (1) and (2), the devices in this thesis *force* the cells to interact with the device surface by a low channel height, and the cells remain bound stronger during washing steps because the cells are attached to two binding surfaces simultaneously instead of one. Other microfluidic devices are discussed in this chapter.

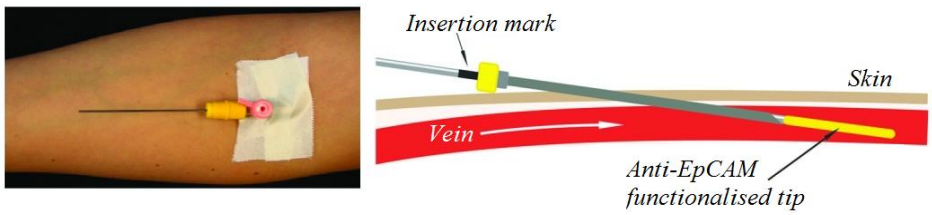

*Figure 4 GILUPI CellCollector, an example of microscale technology, inserted into the patient blood stream (**A**). The tip of the medical wire is functionalised with anti-EpCAM for CTC capture (**B**). Adapted from Saucedo-Zeni et al., 2012.*

Microfluidic device operation methods

There are two main categories in rare cell detection methods from blood samples: static and continuous methods. Static methods simply analyse a sample after which the sample is discarded. Continuous methods operate like a haemodialysis machine (*Figure 5*), in which the device is (externally) placed in series with the patient's blood stream. Generally, the sample volume of static rare cell detection methods is only a few millilitre blood because there is a limit to how much blood can be given by the patient. Continuous rare cell detection methods, however, could be scaled up to large sample volumes (up to 5 L per 24 h) (1) if they are not subjected to fouling, (2) if they do not have a too low volumetric flow rate, and (3) as long as substances from the device do not enter the patient's blood stream. Regarding (1): When the capture surface of the device is covered with biomolecules or cells due to fouling, the cancer cells cannot be captured anymore. Regarding (2): A low flow rate that is too low would require the patient to be connected to the device for too long. Regarding (3): Labelling or capture molecules could be harmful to the patient's health or interfere with disease treatment. (Allan & Keeney, 2010; Biosystems, 2018; Radisic et al., 2006).

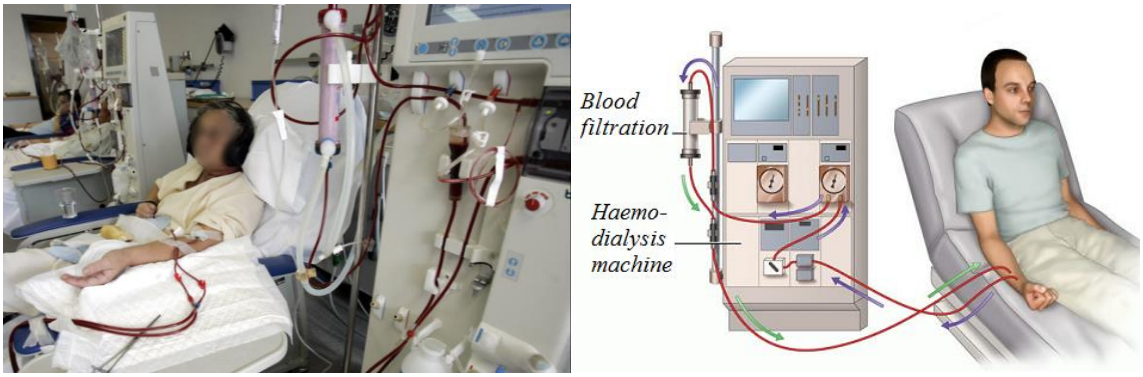

Figure 5 Haemodialysis is an example of continuous operation of blood filtration device. Blood flows from the patient to the machine, in which filtration of toxins and in the future possibly also CTCs, after which the filtered blood flows back into the patient.

Sample enrichment methods

There are two main categories for sample enrichment: positive and negative enrichment. In negative enrichment, all non-target cells are captured and thereby 'removed', leaving only the target cells in the sample. The target cells are hereby less exposed to shear stress because they easily flow through the device (they are 'eluted'). Also, the target cells do not need to be labelled, allowing post-enrichment cell characterisation. In positive enrichment, the target cells are captured while the non-target cells are eluted. The benefit of this method is that a smaller filter surface area is required for the same sample size, because only the rare cells are captured while the bulk of the cells are eluted.

Device operation and sample enrichment in this thesis

As was explained in *The main challenge with circulating tumour cells*, current technologies analyse a small sample of a few millilitres as there are practical and ethical limits to blood sample size (Allan & Keeney, 2010). In many cases, however, this sample volume is too small to detect CTCs. This thesis evaluated the possibility of continuous sampling. Continuous sampling permits only capture of target cells, because non-target blood cells need to be recirculated into the patient blood stream, so positive enrichment was applied.

Examples of positive enrichment microfluidic CTC capturing methods

CellSearch®

An example of a static method is CellSearch®, which is the only FDA-approved CTC enumeration technology. This assay requires 7.5 mL blood from which tumour cells are immuno-magnetically enriched using epithelial cell adhesion molecules, followed by a fluorescent labelling step (output shown in *Figure 6*). The labelling molecules specifically bind to either epithelial cells or leukocytes. The main limitation of this technology is its sample volume. Also, the reported cell recovery show variation: 40% (Harb et al., 2013); 52% (Swennenhuis, Reumers, Thys, Aerssens, & Terstappen, 2013); 71% (Hillig et al., 2015); 82% (Riethdorf et al., 2007). This variation, possibly caused by cell loss during operating steps and its inability to capture cells with low EpCAM expression, makes the device unpredictable. The devices in this thesis force cells to interaction on two sides for increased binding strength, to also capture cells with lower EpCAM expression levels.

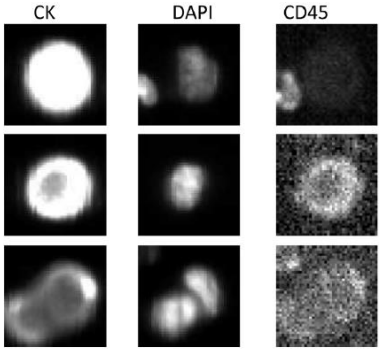

Figure 6 Output of CellSearch® CTC detection with black and white camera. Cells were stained with the epithelial marker pan-cytokeratin (left), the nuclear marker DAPI (centre), and the leukocyte marker CD45 (right). (Hillig et al., 2015)

Isolation by size of epithelial tumour cells (ISET)

The continuous ISET filtration system (RareCell, Paris, France) performs isolation by size using a polycarbonate filter (Pailler et al., 2016; Vona et al., 2000). Epithelial-marker-negative CTCs can be detected and recovered by ISET by size-dependent CTC isolation, because many CTCs are larger than other blood cells (*Figure 2-A*). In clinical tests with several types of carcinomas, the ISET system

showed to be more sensitive in CTC detection with metastatic lung cancer patient samples compared to the CellSearch® system (Farace et al., 2011). In this thesis, like the ISET, large CTCs have more difficulty passing the device (similar to isolation by size). Cell capture that is mainly based on tissue-type specific markers results in more selective capture, *Figure 7* shows presence of red and white blood cells captured by ISET.

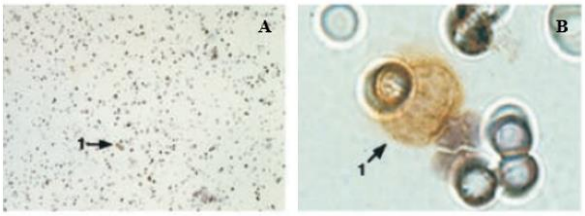

Figure 7 MCF-7 cell (indicated with arrow), surrounded by leukocytes and filter pores, captured from blood in ISET filtration system. Adapted from Vona et al. (2000). (A) 10x magnification and (B) 100x magnification.

High-throughput micro-sampling unit (HTMSU)

A cuboid channel device with similar aspect ratio and antibody binding was able to capture CTC from 1 mL blood in 37 minutes with 97% recovery. The device comprises of 51 channels (Adams et al., 2008) (*Figure 8*). Several geometries were evaluated, and microchannel blockage was observed at a channel height of 20 µm. Increasing flow velocity resulted in the unsolicited cover plate detachment. The channel height of most devices in this thesis was also 20 µm and the devices were operated at high flow velocities. The top glass was immobile by the use of sturdy fabrication method and materials.

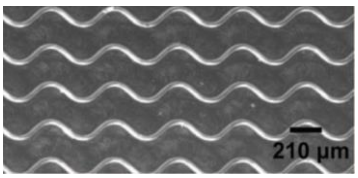

Figure 8 Cell capture region of HTMSU, which comprises of 51 channel per device (Adams et al., 2008).

CTC-chip

A micro-post array optimized for cell-antibody contacts with a throughput of 1-2 $mL.h^{-1}$ (Nagrath et al., 2007). Both cell enumeration and genomic DNA extraction were performed. The micro-posts (*Figure 9*) were coated with anti-EpCAM antibodies.

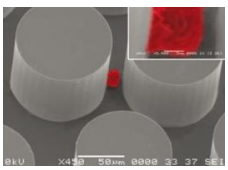

Figure 9 Scanning electron microscope (SEM) image of a captured NCI-H1650 lung cancer cell spiked into blood (pseudo coloured red) (Nagrath et al., 2007).

CTC-Trap

The CTC-Trap is a device evaluated by P.A. Goldsteen (2016, WUR) and comprised two glass slides separated using adhesive tape, with a relatively large surface area due to the channel width and length (12 mm x 50 mm). The antibody coating was the same as the coating in in this thesis. Both single-sided and double-sided functionalisation was possible. A microscope was used to determine cell capture number from a small area of the channel (*Figure 10*).

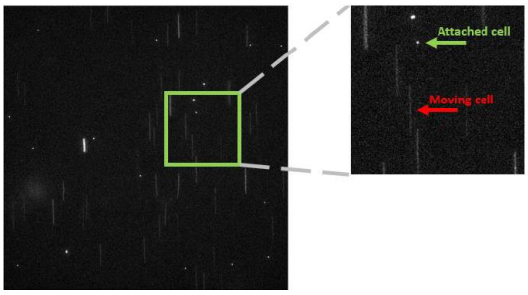

Figure 10 Output of CTC-Trap CTC capture device, obtained by filming a small surface area in the middle of the device.

Table 1 provides additional specifics of the described devices.

Table 1 Comparison of continuous CTC capture assays. [A]: Cell size not mentioned, no negative control used.

Technology	**Geometry type of the channel**	**Dimensions (height x width, µm)**	**Coating**	**Cells (size)**	**Source**
CTC-Trap	Cuboid	25 x 120	Anti-EpCAM	MCF-7 (20 µm), PC-3 (25 µm)	Goldsteen, 2016
HMTSU	Sinusoidal	35 x 150	Anti-EpCAM	MCF-7 (24 µm)	Adams et al., 2008
ISET	Circular	8 x 600	-	MCF-7[A]	Vona et al., 2000
CTC-chip	Micro-post array	100 x 100	Anti-EpCAM	Clinical samples	Nagrath et al., 2007

Research relevance and goals

This thesis is an explorative feasibility study for continuous enrichment of CTCs from whole blood using microsieves. Current FDA-approved method CellSearch® frequently captures 0-10 cells per blood sample. Because of the presence of many (biological) variables (e.g. time and site of sampling), the clinical relevance of a few detected CTC is doubtful (F. A. Coumans et al., 2012). By increasing the sample size, and thereby the number of detected CTCs, CTC enumeration becomes clinically interesting because of improved statistical accuracy. A microsieve that can be operated continuously is proposed to solve the sample-size limitation of other devices, and this thesis evaluates the feasibility of this idea. On top of the improved statistical accuracy, this thesis also aimed at providing clinically and societally relevant research by assessing simple methods for cell detachment without rupturing the cell membrane, often underestimated by other research, because this allows downstream cell characterisation, which is essential for drawing clinically relevant conclusions.

Therefore, the goal of this thesis was to predict how to design and operate such a microsieve by designing, fabricating, and evaluating devices that model a single pore of this microsieve. It was evaluated whether a one millimetre pore depth will yield high cell capture. Properly evaluating this using the microsieve itself will not be possible because direct cell observation will be visually hindered by the array of long pores. The device models in this thesis were each made of one channel with horizontal orientation relative to the microscope for easy cell observation. With these device models, the relation between flow velocity and cell distribution in the channel was evaluated. Also, methods for cell detachment without rupturing the cell membranes were tested. The following two research questions were posed:

(1) At which linear flow velocity are all cells captured within the first 1 mm of the channel?
(2) Under which condition do the captured cells detach from the channel?

Regarding (1): The evaluation of linear flow velocity and cell distribution includes understanding the effect of single versus two-sided functionalisation and the influence of increased channel height.

Regarding (2): Captured cells could be detached and consecutively obtained for further downstream cell characterisation by increasing the drag force (via an increase in flow velocity or eluent viscosity) or via a change in environmental conditions (pH or ionic strength). The latter method is likely the most effect at eluting cells without the destruction of the cell's integrity, which is beneficial for CTC characterisation, suitable therapy determination, and essential to prevent wrongful clinical assumptions. (Ferreira, Ramani, & Jeffrey, 2016) (Plaks et al., 2013).

Theoretical background

In the previous sections, circulating tumour cells and microfluidic devices were introduced. In this section, the processes involved in cell binding and cell release are introduced. Following, the implications of these processes for optimal device design are given. But first, factors that are important to note when translating CTC capture from laboratory setting to the clinical setting are discussed.

Biological considerations

There are biological factors need to be considered before clinical conclusions can be drawn based on the presence or absence of CTCs. These factors are discussed in this section.

Size heterogeneity

CTCs from different tumours are diverse in size (Hosokawa et al., 2013), so not all cells are forced against the top and bottom antibody coating of the microfluidic devices in this thesis, which is one of the benefits of the employed device design. The device design (channel height) might need to be adjustable for clinical use, depending on the size of the tumour cell of interest. Alternatively, the device needs to consist of a range of different channel heights via multiple channels or a channel with a height profile to capture cells from a heterogeneous clinical sample.

Antigen heterogeneity

Caution needs to be taken for affinity-based capturing methods because of surface marker heterogeneity of circulating tumour cells (Schwab, 2011). While antigen expression of established cell lines is stable (Fargion et al., 1986; Konigsberg et al., 2011), antigen expression of *in vivo* tumour cells is dependent on tumour type, disease stage, tumour microenvironment, and host anti-tumour immunity (Baeuerle & Gires, 2007). On top of this, a tumour can be genetically unstable which could result in the partial loss of surface marker genes at a certain point in time (Barteneva et al., 2013; Deelstra, 2017; Farace et al., 2011; Perry, Thomy, Das, Coffinier, & Boukherroub, 2012; Plaks et al., 2013; Wang et al., 2016). For example, epithelial to mysenchymal transition (EMT) is the loss of epithelial markers by genetic mutations (Strati et al., 2013). Because of this phenomenon, affinity-based capture methods (which are relying on the presence of epithelial markers) could miss phenotypically heterogeneous cells when these markers are lost. Other antibodies besides anti-EpCAM, or a cocktail of antibodies, could target other markers that are not yet lost, depending on the degree of EMT.

Coagulation of CTCs

Epithelial cells tend to adhere to surfaces and other cells. Cell clumps experience a larger shear stress in the channel due to their larger size compared to individual cells. In the laboratory, cells are usually harvested using trypsin (serine protease) to break the peptide bonds between the cells and their surface and ethylenediaminetetraacetic acid (EDTA) as a chelator for calcium to break cadherins to prevent cell-cell adhesion (Takeichi, 1988). Patient blood could contain tumour clumps, so the device performance needs to be evaluated for such clumps.

Whole blood samples

Affinity-based filtration methods need to be tested with whole blood samples to evaluate their performance with the presence of platelets or coagulating factors and the absence of anticlotting factors. Platelets and coagulating factors can cloak the target cell's surface, preventing the attachment of these cells to the antibody-coated surface (Plaks et al., 2013). Also, it was hypothesised by Goldsteen that in the CTC-Trap the red blood cells sediment faster than CTCs and thereby inhibit the CTCs from reaching the antibody-coated surface. The devices in this thesis employed a small channel height be more sure the CTCs interacted with the antibody-coated surface and sedimentation was prevented by adopting high flow velocities.

Classification of noncancerous epithelial cells as CTCs

Patients with various benign inflammatory colon diseases harboured viable circulating epithelial cells, whereas healthy subjects did not (Pantel et al., 2012). CellSearch® assay classified these cells as CTCs. Circulating noncancerous epithelial cells could originate from healthy tissue and benign tumours and are thereby not relevant in the prognosis prediction (Plaks et al., 2013). This stipulates the importance of downstream cell characterisation to distinguish between cancer cells and benign cells.

Seeding potential of CTCs

Not all circulating tumour cells will result in secondary tumours ('CTC seeding'), as they might not survive their environment due to the presence of natural killer cells (NKc) or the absence of nearby tumour cells or growth promoter molecules. An estimate was made that 0.01% of the circulating tumour cells is able to form a secondary tumour (Langley & Fidler, 2011). Clinical studies are therefore required before conclusion can be drawn regarding the device's relevance.

Sample site(s)

Some circulating tumour cells might not travel far from the primary tumour and thereby never reach the blood sample site(s) due to cells getting stuck in blood capillaries, kidneys, or the liver. The site of blood collection is therefore important in a clinical setting (Plaks et al., 2013). Not all blood vessels can act as a 'minimally invasive blood sample site'. Also, the tumour could spread via the lymphatic system instead of the peripheral blood stream (*Figure 11*). Metastatic disease could thusly arise without the detection or even presence of any circulating tumour cells in the blood when sampling from only one site. Large sample collection (possible via continuous operation) from multiple sites would be ideal for biological and statistical accuracy.

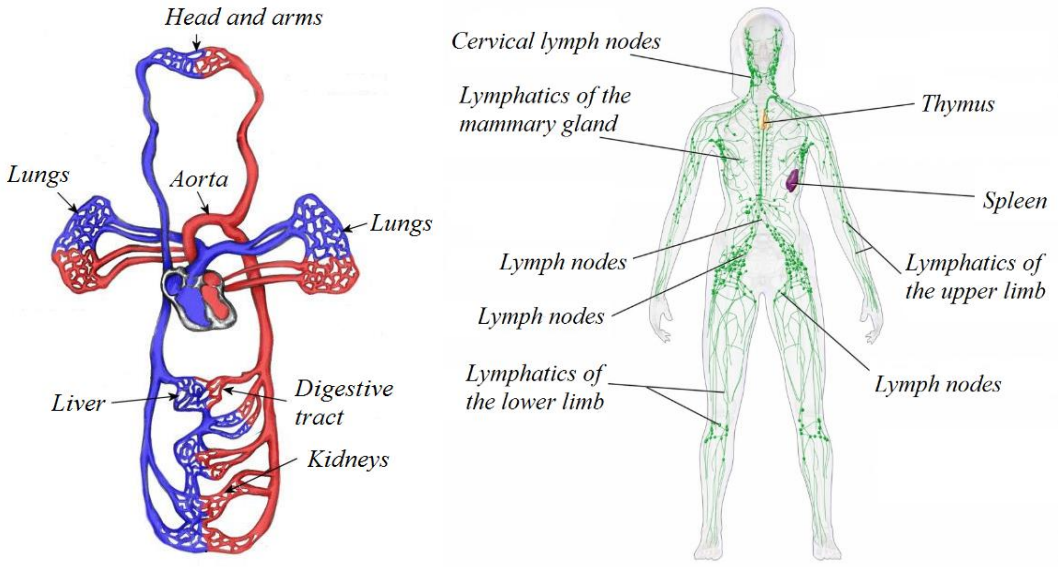

Figure 11 (A) The blood circulatory system and (B) the lymphatic circulatory system. (A) Adapted from Teachpipe.com staff (2018), ''Circulatory system'', http://www.teachpe.com/anatomy/circulatory_system.php. (B) 'Lymphatics' is short for 'lymphatic vessels'. Adapted from Blausen.com staff (2014), ''Medical gallery of Blausen Medical 2014'', WikiJournal of Medicine 1 (2).

Processes involved in cell capturing

Introduction

This section introduces forces that are involved in the capturing process of cells in a microfluidic channel and concludes with the implications of these forces for the design of the device. For this thesis, the relevant direction of cell movement by these forces is in the vertical plane, because only the top and bottom sides are coated with antibodies. This review is relevant because of laminar fluid flow inside the microfluidic channel. In a laminar flow profile, the cells remain at a constant distance from the wall, as was observed in preliminary observations in this thesis with vinyl glue devices which have imperfect walls. With laminar flow, cells might never interact with the walls and thereby not be captured. The following forces that might cause the cell to migrate towards or away from the antibody-coated surfaces are discussed: channel height, local deviation of laminar flow, shear-gradient induced lift, wall interaction force, diffusion, and sedimentation.

Important notes

The antigen-antibody bond strength is a parameter that is only relevant for cell detachment, not for cell attachment. This appears counter-intuitive, but the conditions under which binding is facilitated (e.g. a slow flow rate) are much milder than the conditions required to break the formed antigen-antibody complex. The limiting factor in cell capturing rate is therefore not the binding strength, but the time it takes before a cells successfully encounters the antibody layer. The longer this takes, the further away from the entry the cell is captured.

Channel height

With a channel height equal to the cell size, the cells are forced to interact with the sides, so no migration of cells towards the sides is required (*Figure 12-B*). The forces discussed in the next sections are relevant for devices with a channel height larger than the cell diameter (*Figure 12-C*).

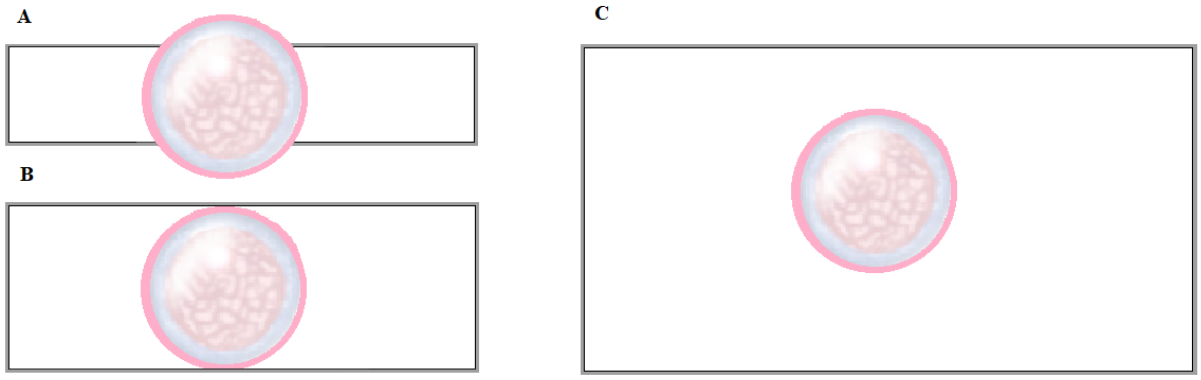

Figure 12 Simple representation of the channel entry of (A) a channel with a height smaller than the cell's diameter, (B) a channel with a height equal to the cell's diameter, and (C) a channel with a height larger than the cell's diameter.

Disruption of laminar flow

The small Reynolds number (*Re* < 1) of the channels mean the fluid flows through in a laminar flow profile, also called streamline flow. The fluid flows orderly in parallel lamina without the presence of eddies (swirling of fluid); the exact opposite of turbulent flow. Bound particles locally disturb the flow profile (*Figure 13*, especially when a large cell is bound inside a microchannel. This disruption of laminar flow can result in a localised turbulent flow, allowing the cell to hit the wall. Early microscope observations in this thesis indicated that cells are not disengaged from the original flow line during and after passing a stagnant particle: they maintain the constant distance from the wall. This force might therefore be negligible.

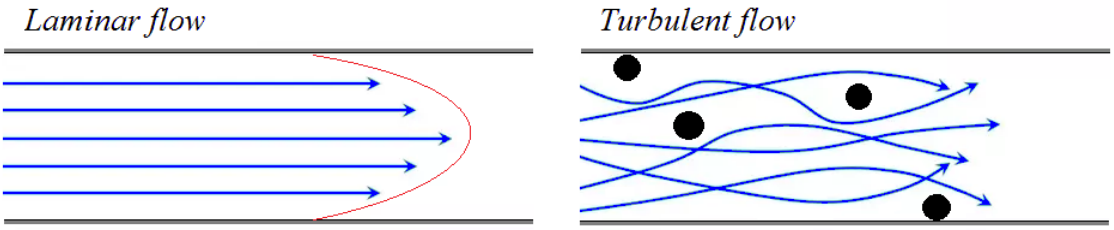

Figure 13 Laminar flow profile (top image) and the possible localised disruption of laminar flow by stagnant cells (black dots, bottom image). The lines represent flow lines of the fluid. The red line shows the parabolic flow profile of laminar flow.

Shear-gradient induced lift

It is assumed the fluid has zero velocity near the stationary boundary (no-slip boundary condition), and maximum velocity in the middle of the channel. The no-slip boundary condition is caused by a stronger adhesion of fluid molecules to the stationary wall molecules compared to the cohesion between the fluid molecules. This creates a parabolic velocity profile (*Figure 13*). In turn, this profile creates a shear gradient across the cells surface, because the flow velocity of the fluid relative to the cell is not the same on every point of the cells surface. This causes the cell to be directed to the side with the largest relative velocity: to the wall (*Figure 14*).

This force is largest at largest velocity gradient, i.e. in the 'developed region' of the channel; the velocity gradient is small or even zero in the 'entrance region' (regions shown in *Figure 15*). It was calculated that this entrance region is negligible short because of the small Reynolds number. This force is in the direction of the sides and quantitatively the most significant of the forces described in this section (Martel & Toner, 2014; Zhang et al., 2016). Still, it was calculated (formulas provided by J. Baggerman) that by shear gradient induced lift force the cells migrate only 2×10^{-8} m during a 10 second residence time in the channel.

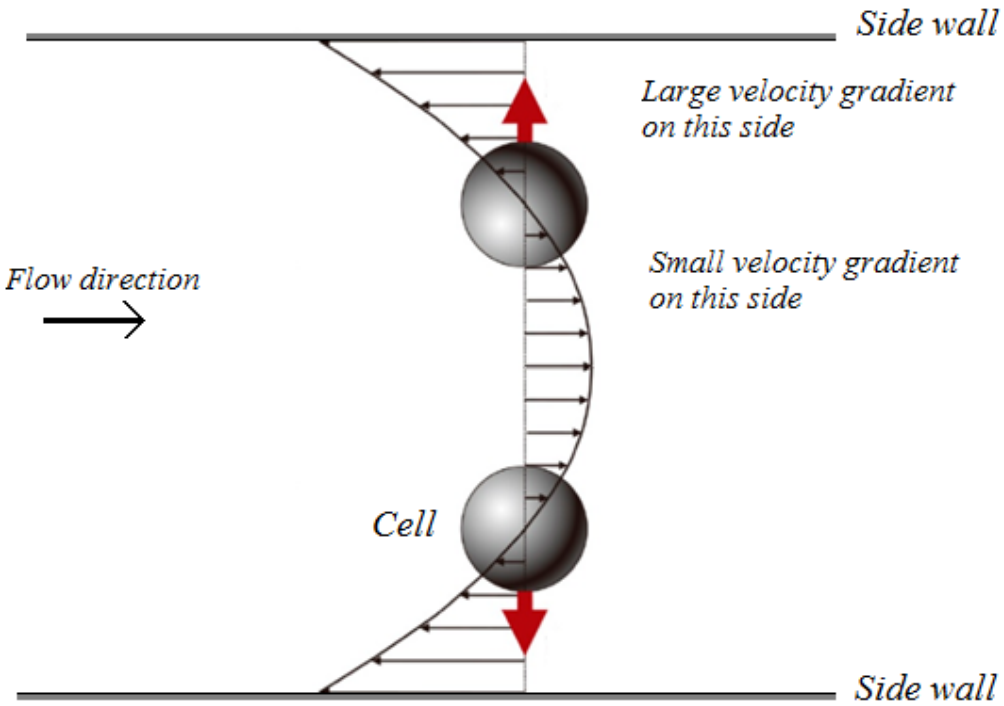

Figure 14 Fluid flow velocity profile relative to the velocity of the cell and the direction of the shear-gradient induced lift force is indicated with red arrow. The relative velocity difference between cells and flowing fluid is shown by the arrow length and direction. The fluid flows at almost the same velocity as the cell in the middle of the channel. At the sides of the channel, the fluid velocity is small due to no-slip condition, so the velocity difference with the cell is large. This causes a pull on the cell, and the cell migrates towards the side. Adapted from Liu, C. & Hu, G. (2017).

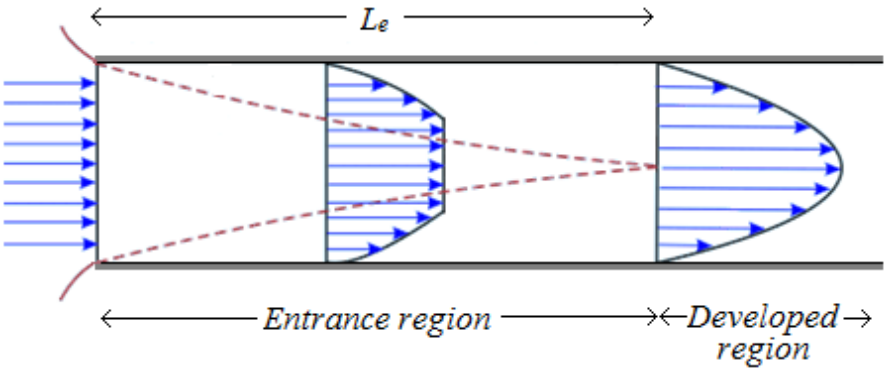

Figure 15 Parabolic flow profile at the developed region, but not at the entry region, which shows a rectangular flow profile. The L_e value was calculated to be negligible short. Adapted from nptel.ac.in staff (no date), retrieved 25-06-2018, http://www.nptel.ac.in/courses/Webcourse-contents/IIT-KANPUR/FLUID-MECHANICS/lecture-31/31-1_entry_flow.htm.

Wall interaction effect

The wall interaction effect is a force on the cell directed away from the wall. This 'wall effect' is caused by an increase in pressure when the cell approaches the wall, because the fluid flow is constricted between the wall and the cell when this happens (Liu & Hu, 2017). An equilibrium can be reached between the wall effect (which increases in size when decreasing distance to the wall) and shear-gradient induced lift (which also increases with decreasing distance to the wall by an increase in velocity gradient). This is the inertial equilibrium position of the cell and additional reason the shear-gradient induced lift force is not contributing to the migration of cells to the antibody-coated surface.

Diffusion

Diffusion is the random motion of single particles. The mean square distance that a particle diffuses in time t is: $\langle r^2 \rangle = 6 \cdot D \cdot t$, where D is the diffusion coefficient. According to the Stokes-Einstein relationship, the diffusion coefficient is given as: $D = (k_B \cdot T)/(3 \cdot \pi \cdot \mu \cdot a)$, where a is the size of the particle. Calculating this showed that diffusion can be neglected. (Zhang et al., 2016).

Sedimentation

Although a rather slow process, gravity could be used to sediment the cells onto the bottom glass plate. This effect is most prominent under slow flow velocities. The direction of this force is towards the bottom side of the devices in this thesis but could be perpendicular to the channel surface of the future microsieve device. Goldsteen described that sedimentation of red blood cells should give rise to improved binding of MCF-7 cells at the top side of the device, but this was not observed.

Binding rate as a function of flow velocity

The formation of enough antigen-antibody complexes for cell capture depends on the relative velocity. The relative velocity is defined as the velocity of the antigens on the cell relative to the antibodies on the surface, which are stagnant. A faster flow velocity results in a decreased binding rate. (Chang & Hammer, 1999). The binding rate is the number of formed antigen-antibody complexes per unit of time.

When decreasing the flow velocity by tuning the flow equipment is not sufficient (for example in this thesis), the velocity can be decreased further by increasing the viscosity of the sample (patient blood). Intravenous solutions may contain hydroxyethyl starch (HES, brand name Voluven), which is non-ionic maize starch derivative used as volume expander or plasma substitute in case of severe blood loss (Mutter, Ruth, & Dart, 2013). This product could be used to simulate blood viscosity in a research setting without altering the ionic conductivity or be used in a clinical setting to temporarily increase the blood viscosity for improved cell capture. Note that increasing the viscosity also increases the drag force experience by captured cell, which could induce cell detachment.

Summary on cell attachment and design implications

Many devices described in literature require slow velocities to capture cells. Employing a slow velocity is not in line with the goal of this thesis to operate a device with high throughput, which increases with increasing flow velocity. To overcome this via proper device design, the forces that are involved in cell migration to the walls were evaluated. Diffusion was calculated to be negligible. The wall-effect is a force directed *away* from the wall. Sedimentation by gravity does not induce cell movement in the direction of the sides in the future microsieve device. The shear-gradient induced lift is usually the largest force of the mentioned forces, but it was calculated that this force is negligible and could even be fully overcome by the wall interaction effect. Therefore, it was chosen to *force* the cells to interact with the antibody coating by employing a channel height equal to the size of the average cell. This means a channel height of 20 µm was employed in three of the four devices, and one device with a 30 µm channel height to verify the predicted decreased binding rate in devices with a large channel height.

Processes involved in cell detachment

Introduction

After CTC enrichment from blood, the future microsieve device will be disconnected from the patient and the captured cells need to be detached and consecutively obtained in a controlled fashion for enumeration and downstream cell characterisation. To detach bound cells, the drag force can be increased, or the environmental conditions can be changed. Note that after successful binding, it is assumed that the cells will remain bound when the conditions in the channel are not altered because the release conditions are less mild than attachment conditions. The conditions under which cells are released from the channel are discussed in this section.

Drag force increase

As described by Stoke's Law for frictional force, the viscous drag force (in N) experienced by captured cells (which causes detachment from the coating) can be increased by increasing the flow velocity or the viscosity of the fluid:

$$F_{drag} = 6\pi \cdot \eta \cdot R \cdot v$$

with η the dynamic viscosity in Pa.sec, R the radius of the particle in m, and v the fluid flow velocity relative to the particle in m.sec^{-1}.

The antigen-antibody complex will be broken above a certain drag force: $F_{drag} > F_{bond\ strength\ of\ Ag/Ab\ complex}$. However, a study at the University of Twente found that increasing the flow velocity ruptures the cells before the complex dissociates. Possibly the cell membrane at the surface experiences no drag force (because the fluid flow velocity is assumed to be zero at the surface) while the membrane on the channel side is exposed to shear stress by flowing fluid. Another option is that the complex bond strength is stronger than the membrane integrity in general. (Di Carlo, Irimia, Tompkins, & Toner, 2007; Goldsteen, 2016; Martel & Toner, 2014).

Cell detachment by local increase in fluid flow

In this thesis, a constant pressure gradient is chosen to operate the devices, to keep the drag force experienced by the cells constant: the cells are pulled with a constant force through the channel. The pressure experienced by the cells remains the same, while the fluid velocity adapts while cells bind and fill the channel. Another way to operate the devices, is to set a constant overall flow rate. This might, however, result in an increase in local flow velocity over time: when cells are captured in the channel, the available space for free fluid flow is decreased while the overall flow rate is not affected. By this increase in local flow velocity, cells that were captured could detach.

Change of environmental conditions: pH and ionic strength

Increasing the drag force or shear stress could rupture cells which makes enumeration and downstream cell characterisation impossible. Therefore, releasing cells by selectively breaking the antigen-antibody complex bond by a change of environmental conditions is a more elegant method. Antigen-antibody bonds are non-covalent and reversible, and formed by a combination of hydrogen bonds, hydrophobic interactions, electrostatic and Van der Waals forces. An example: immunoglobulin G (IgG, a type of antibody) binds to neonatal Fc receptor at pH 6.0-6.5 (in endosomes) but releases again at pH 7.0-7.4 (cell surface) (Chan & Carter, 2010; Raghavan, Bonagura, Morrison, & Bjorkman, 1995; Rodewald, 1976). Because IgG's are well-studied, we know that the histidine residues contribute to the pH dependence of the affinity (Carter, 2006; Raghavan et al., 1995). Molecular knowledge on the specific interaction between the antibody anti-EpCAM and antigen EpCAM is missing. Also, the effects of temperature (in case of e.g. hydrogen bonding) and salt concentration (ionic strength) on binding strength of anti-EpCAM and EpCAM complex are not known.

Knowing these effects might become important in a clinical setting, because the attachment and detachment process should remain predictable while knowing the blood parameters. This is important for the confidence level of the circulating tumour cell enumeration and thereby important for the disease (progress) diagnosis.

Dissociation rate

The dissociation rate of the antigen-antibody complex is finite, implying cells could detach due to random dissociation of the complex. Yet, each cell in bound to the device surface via a multitude of antigen-antibody complexes. The dissociation of all these complexes at the exact same time is unlikely, so random dissociation is not expected to play a significant role in cell detachment. Each cell contains many thousands of EpCAM antigen on their surface (Yao et al., 2013).

Trypsin

Trypsin is a hydrolysing protein that is widely used to release cells from surfaces. Trypsin could be employed to dissociate cells from the channel by cleaving surface protein peptides on the C-terminal side of lysine and arginine amino acid residues. It was observed that trypsin alters the proteome of cells during cell culture; amongst other cancer-regulating protein expression was modified (Huang et al., 2010). Trypsin was used by Adams et al. (2009) in the HMTSU chip for cell release, though a 10-minute waiting step had to be employed for cell detachment from the coated surface. A faster methods that still allows tumour cell characterisation after capture is ideal.

Summary on cell detachment

Each captured cell will be attached to the antibody layer via multiple antigen-antibody complexes. Because of a velocity difference of a captured cell and the moving fluid, the cell experiences drag force. To detach the cell, this drag force can be increased by increasing flow velocity or fluid viscosity, but these methods are considered destructive for the cell's integrity. The influence of environmental parameters (pH and ionic strength) on EpCAM antigen and anti-EpCAM antibody are not yet fully described in literature. Investigating this is worthwhile as it improves cell attachment prediction accuracy and allows intact release of captured cells for downstream characterisation.

Rationale behind device design and fabrication

Introduction

In previous sections, the problem definition (cancer death rate) was stated and several CTC detection devices were described. A too small sample size was proposed as the main limitation of current analytical technology. A theoretical background of processes involved in cell capture and release was provided. The goal is to design device model for a future microsieve, so this device is introduced in this section. Also, design restrictions posed by fabrication limits are explained. Finally, the implications of all this information on device design and operation are given.

Future microsieve device

This microfluidic device will be a silicon-based membrane comprising of a multitude of pores that each have a depth of one millimetre, a width of 200 µm, and a height 20 µm. The full inner surface of the pore will be coated with antibodies. The device will be connected in series with the patient blood for continuous operation with a throughput of 5 litres in 24 hours.

Fabrication methods

Photolithography is a technology with which a channel or pore can be created by exposing light-sensitive photoresist layer to UV (ultra violet)-light. UV-light either solubilises or insolubilizes the photoresist, which locally exposes the substrate below. Next, a series of chemical treatments etches away the substrate, creating the channel or pore (*Figure 16-A*). Direct fabrication of the channel via photolithography is not possible, too expensive and/or too time consuming, because of the required channel length (obtained by etching) is in centimetre scale while the other dimension require ±1 µm precision. The etch direction and shape is theoretically possible via dry anisotropic etching (*Figure 16-D*).

The require channel dimensions are 200 µm x 20 µm x 15 mm. The devices were therefore made indirectly from photolithography: this technology was used to create a precise mould (*Figure 16-B*) that was consecutively used in soft-lithographic device fabrication. Soft lithography is a technology in which ‘soft’ elastomeric materials are used for replicating structures. The materials used are polydimethylsiloxane (PDMS) and epoxy resin.

PDMS is an optically clear, inert, non-toxic elastomer that remains flexible upon curing. It is the product of PDMS resin (polydimethylsiloxane) and a cross-linking agent. Epoxy is the cured product of an epoxy resin (polyepoxide) and a polyamine harder. Spacers are plateaus on a surface on which a plate can be placed, creating a channel in between the spacers.

This figure (*Figure 16-A, B*) depicts the problem of too long channel length for direct device fabrication with photolithography, and the solution to this: fabricating a mould that could be used in soft lithography with PDMS and epoxy resin.

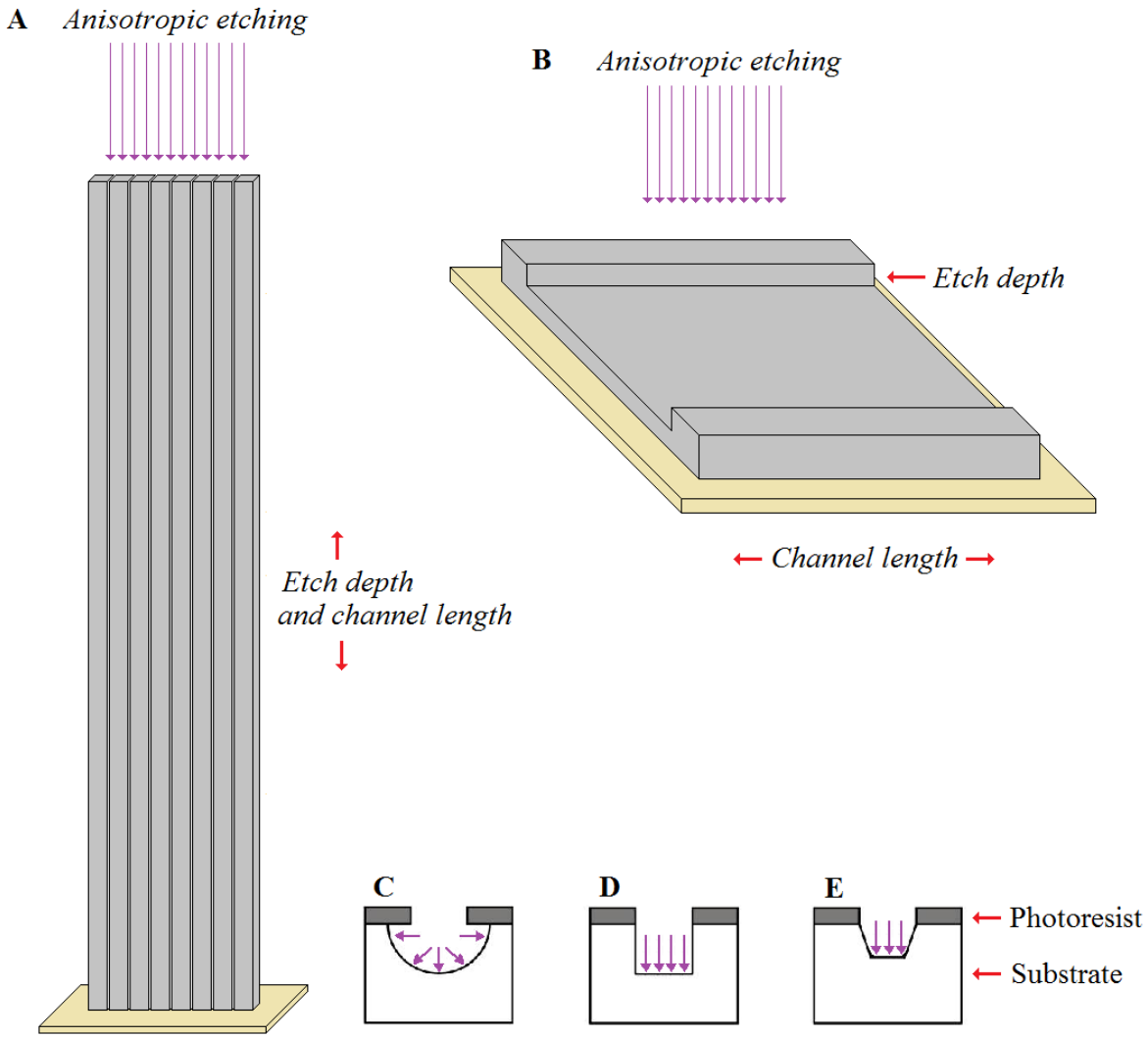

Figure 16 Photolithographic method for (A) direct device fabrication, in which the created pore depth (channel length) using etching is equal to the etch depth (for which there is a limit due to UV penetration and costs), and (B) indirect device fabrication; a mould was made that was used for soft lithography. The channel length and etch depth are not linked anymore. The depth (channel length), width and height are to scale in (A) for a device with the dimensions 1.5 cm x 200 µm x 20 µm. The width and height are to scale in (B) for a device with the same dimension but a different length. Etching profiles generated with (C) isotropic etching, (D) dry anisotropic etching, and (E) wet anisotropic etching, adapted from (Betancourt & Brannon-Peppas, 2006)

Channel height

To be sure the cells interact with the antibody-coated surface, the channel height is in the same order as the average cell size (20 µm). With this height, many cells will bind to the bottom as well as the top side, which increases the total cell binding strength with the antibody-coated surface. A smaller channel height is likely to induce clogging (*Figure 17-A*). A larger channel height does not have the benefit of two-sided bonding and allows cells to travel through the channel without at some point encountering the antibody-coated surfaces (*Figure 17-C*).

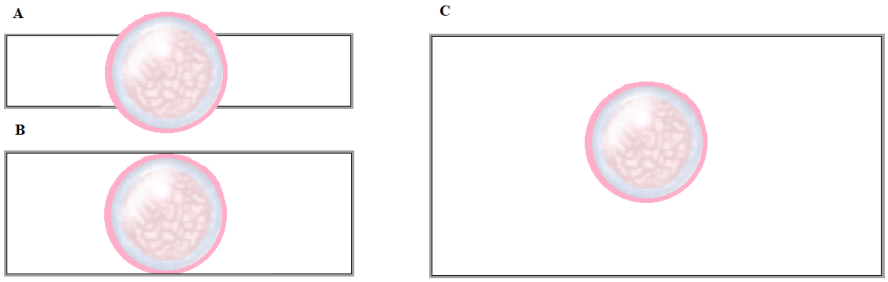

Figure 17 Simple representation of the channel entry of (A) a channel with a height smaller than the cell's diameter, (B) a channel with a height equal to the cell's diameter, and (C) a channel with a height larger than the cell's diameter.

Channel width

For a channel with a height and width equal to the size of a cell, cell capture would produce a large pressure drop due to obstruction. Pressure drop is the difference in pressure between the entry and the exit region of the channel. If a cell obstructs the channel (*Figure 18-A*), one side of the cell will be exposed to the pressure gradient created by the vacuum pump, while the other side experiences ambient conditions. This is unwanted, because it could cause cell rupture, after which the cell cannot be enumerated nor analysed anymore. Therefore, a channel with low aspect ratio (AR = channel height/channel width) was designed. The relatively wide channel allows free fluid flow along attached cells and a lower pressure drop across the channel. *Figure 18-A* shows that a channel with high AR is easily obstructed by the capture of a single cell, and *Figure 18-B* shows that fluid can freely pass the captured cell.

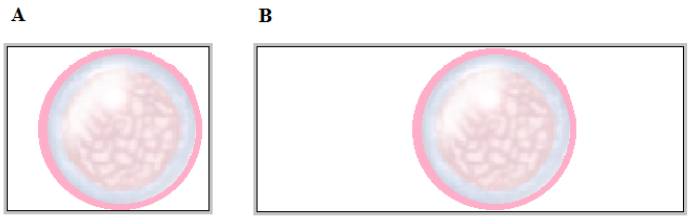

Figure 18 Channel with (A) high aspect ratio (AR = height/width), and (B) low AR.

The long and wide channel dimensions create a large surface area available for cell capture. In epoxy model IV, only the epoxy surface was not surface modified, meaning that 91% of the total inner surface area was coated with antibodies, making it a proper model for a 100% surface area coated microsieve. The coated surface area of the other model devices are listed in *Table 2*.

There is a limit to the maximum channel width, because a width of several millimetres is likely to induce sedimentation of CTCs and blood cells by the formation of stagnant areas. Goldsteen observed variation in detach velocities (a variable depending on the antigen-antibody bond strength) in certain regions in a channel of a 25 mm wide channel. A possible explanation of this was the sedimentation of red blood cells which inhibited the tumour cells from encountering the antibody coating of the device.

Channel length

The future microfluidic device will have a maximum pore depth of one millimetre, and it is important to know under which conditions the cells are most likely to attach within this one millimetre. The model devices can be used to determine at which flow rate the furthest captured cell is still only one millimetre away from the channel entry. A long channel length has more room to find relations between operating conditions and attachment region.

Channel start line

Having a well-defined channel start line is important for quantifying the attachment region of captured cells. If this start line is not well-define or not clearly visible, the travel distance of a cell before it is captured cannot be determined. Images of the channel start lines of different devices are shown in the results section.

Streamlines at the channel start

This thesis aims to model a single pore of the future microsieve device. The way of fluid entering the channel is most similar in epoxy device models, shown in *Figure 19* which shows cross sections of the different device models and how cells approach the channel. Both side views and top views are presented. The top view and side view of the future microsieve pore are schematically identical.

Modelling the correct streamlines of cells that are approaching the channel is important for determining the cell distribution, because it is predicted that these streamlines can have an effect the location of the cell upon entering the channel. In turn, this might influence the final cell capture region.

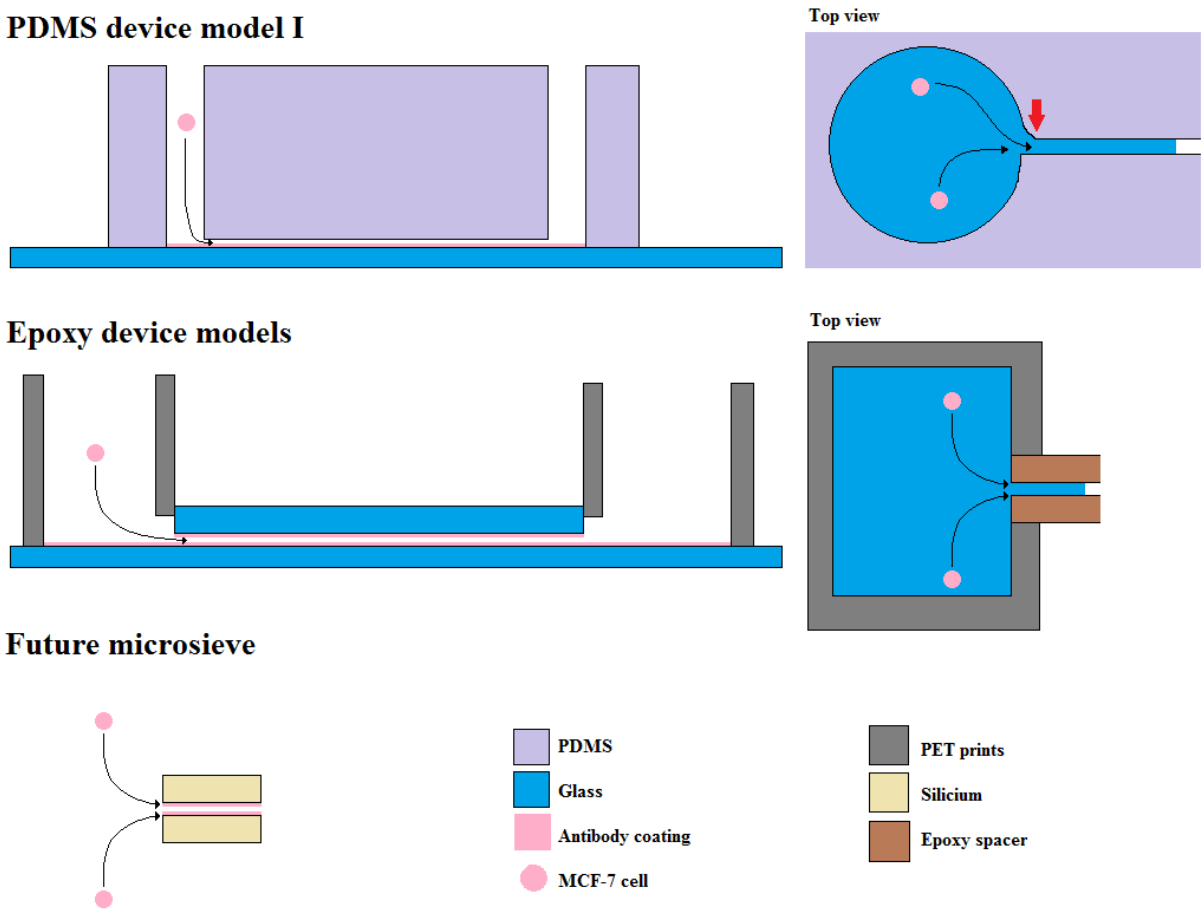

Figure 19 Schematic representation (not to scale) of a streamline of the cell that enters the different devices. The red arrow indicates the presence of microstructures from the mould that was sometimes observed.

Model device description

Devices are depicted in *Figure 20* and *Figure 21*, and their geometries listed in *Table 2*.

PDMS model device I had a semi-circular channel with a maximum channel height of 30 µm. Because of the height of 30 µm, we could evaluate the effect of not forcing the cells to interact with the antibody layer. It was expected that cells are bound less strongly to the antibody layer, so the cells that experienced largest drag force (the largest cells) would detach the earliest.

PDMS model device II was very wide and contained pillars of 4 µm in diameter every 50 µm over its full surface, so it is a micro-post array device. This wide channel was used to decrease the linear flow velocity and to evaluate the formation of stagnant areas.

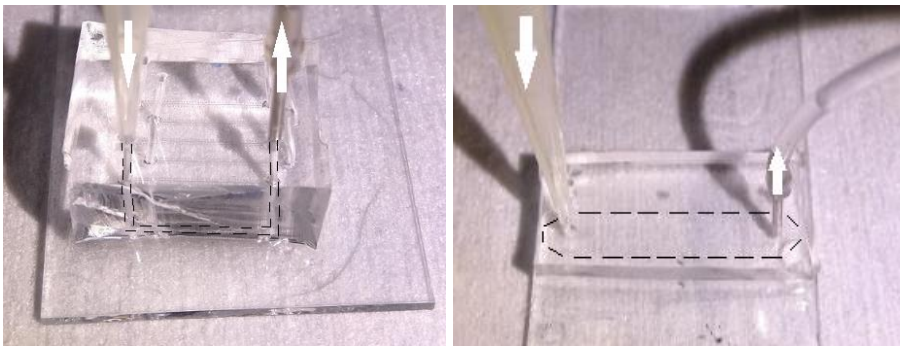

Figure 20 Images of PDMS model devices I (left image) and II (right image). The white arrows indicate the flow direction from reservoir (a pipette tip) to exit tubing via the channel (indicated with black dashed lines). A glass slide is 26 mm in width.

Epoxy model devices III and IV are practically the same, except for the top glass slide, which is either regular glass (model III) or polyacrylic acid (PAA) functionalised glass (model IV). The functionalised glass slides can be coated with antibodies. They resemble the future microsieve device better than PDMS model device I, but they require more steps for fabrication (see Materials and methods section). The low channel height forced the cells to interact with the top and bottom surface simultaneously. It was expected that the effect of earliest elution of large cell would not hold anymore: the larger the cell, the larger the drag force, but also the larger the more tightly the cell is compressed in between the top and bottom surface. Large cells are be able to interact with the top and bottom side simultaneously, while smaller cells are not. It is also expected that a two-sided functionalisation decreases the ease of cell detachment, because the total cell binding strength with the antibody-coated surfaces is higher compared to a single-sided functionalisation.

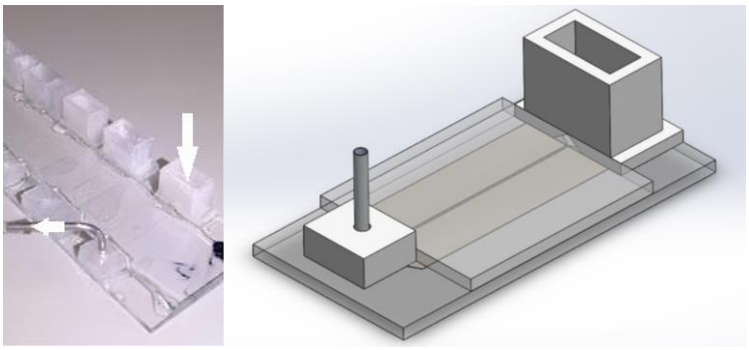

Figure 21 Epoxy model devices with several devices placed on one glass slide (left image) and the design of an individual device (right image, SolidWorks). The largest block is the entry reservoir. The fluid flows through the channel to the exit and leaves via the metal pin to the vacuum pump.

To summarise, the combination of the following characteristics that were predicted to contribute to the success of epoxy device model IV were employed in the device design:

(1) easy cell observation with bright-field microscopy;
(2) well-defined channel starting line for cell distribution determination;
(3) a channel height equal to the average cell size in combination with top-and-bottom functionalisation for doubling total cell binding strength with the coating;
(4) high aspect ratio for prevention of pressure drop and for a large total antibody-coated surface.

The limitations of this device were the small total throughput because the device comprises only one channel, and the requirement for soft-lithographic fabrication using a photoresist mould. The future microsieve device will comprise multiple pores to increase the total throughput and the microsieve can be fabricated directly using photolithography.

Table 2 Geometry of the four model devices used in this thesis.

Device	**Pore geometry**	**Length (cm)**	**Width (µm)**	**Height (µm)**	**Functionalisation surface area**
PDMS model I	Semi circular	0.9	200	30	Single sided, 51%
PDMS model II	Cuboid	2.0	3900	20	Single sided, 50%
Epoxy model III	Cuboid	1.5	200	20	Single sided, 45%
Epoxy model IV	Cuboid	1.5	200	20	Two sided, 91%
Future microsieve	Cuboid	0.1	200	20	Four sided, 100%

Materials and methods

PDMS fabrication

Centrifuged PDMS (10:1 polymer resin/cross linker, Sylgard®184 LOT 0009295924, Farnell, Utrecht, The Netherlands) was poured onto photoresist moulds fabricated in the MESA+ cleanroom with conventional photolithography (Henniker-Plasma, 2017; Keum, Park, & Kim, 2018), which was then degassed in a desiccator and cured for 25-35 minutes at 80 ºC to form a solid PDMS structure. The PDMS structures was manually punched with a 1.00 mm biopsy punch (Harris Uni-Core, Whatman, UK), and cleared from dust with adhesive tape and washed 3x with ethanol. Regular glass sides (RS Components SAS, Beauvais, France) were cleaned with acetone, ethanol, and brushing with a toothbrush (PLUS, Almelo, The Netherlands) under running demi water. PAA-functionalised glass slides were cleaned by sonication in MQ water for 1 minute.

PDMS model devices I and II

Geometric differences between devices are indicated in *Table 3*. Each device consisted of two to six channels. The fabrication steps are depicted in *Figure 23*. The structures for PDMS model devices I and II were treated with oxygen plasma for 120 seconds (Pico, Diener Electronic, Germany) for improved bonding performance to prevent premature device failure (Henniker-Plasma, 2017; Tan, Nguyen, Chua, & Kang, 2010), dropped on a cleaned glass slide and left for about 5 minutes, sealing the edges with additional PDMS, followed by a 4 hour- or overnight curing step in the oven at 80 ºC (kept minimal when using PAA-functionalised slides). Tubing was connected to the structure using 20-gauge (0.81 mm) precision tip (Nordson EFD, USA). A gel loading pipette tip functioned as entry reservoir (*Figure 17*).

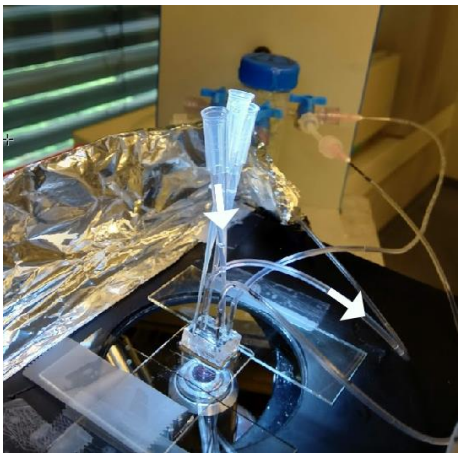

Figure 22 Pipette tips are the reservoirs in PDMS model device I. The arrows indicate the fluid flow: from the reservoir, through the channel, into the tubing to the vacuum pump.

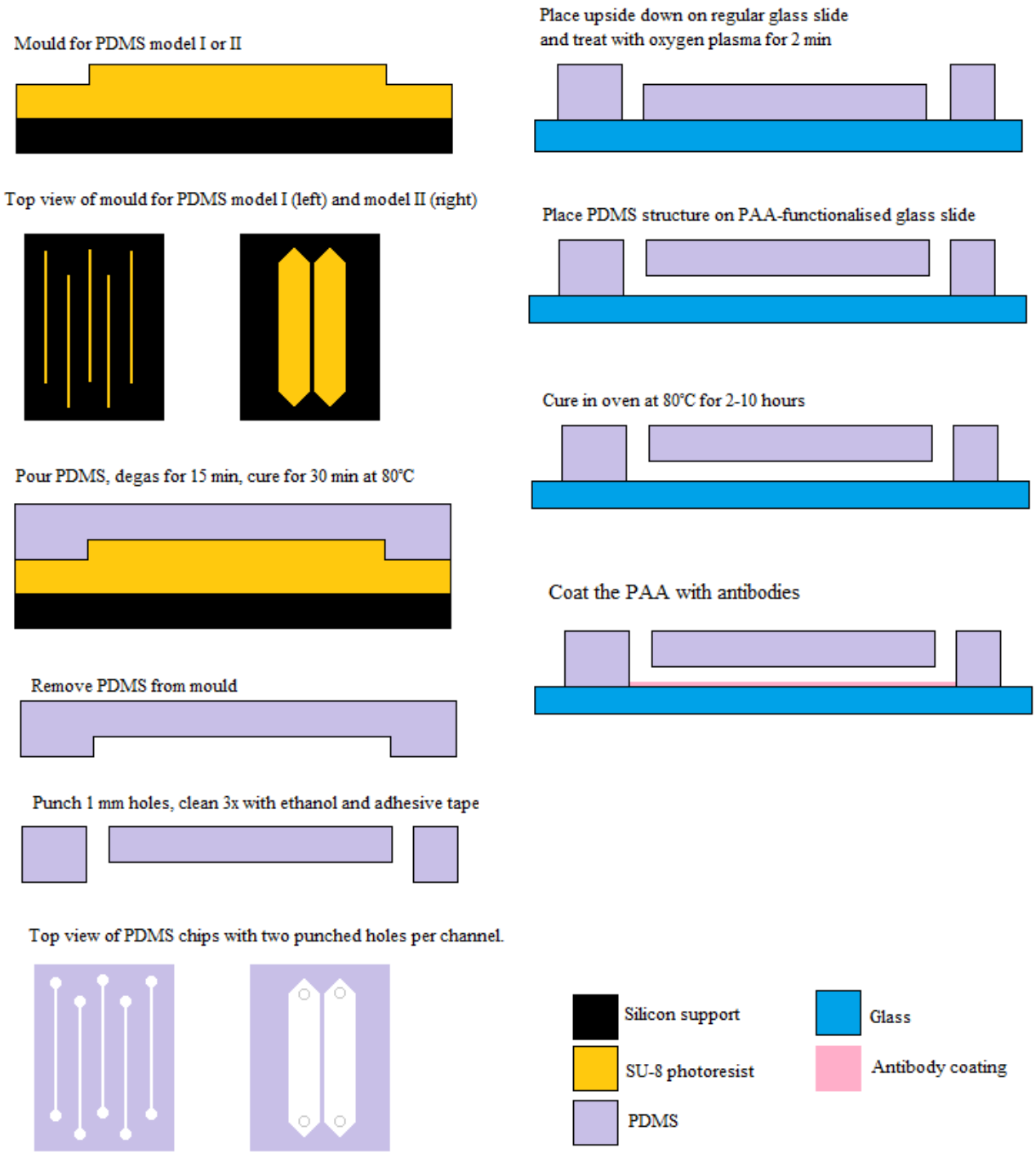

Figure 23 Schematic side-view (unless otherwise indicated) fabrication scheme for PDMS model devices I and II. PDMS device model I and II differ in the used moulds and thereby the channel geometries.

Epoxy model devices III and IV

The epoxy models differ in single- or two-sided functionalisation with antibodies. Each device consisted of one channel. The fabrication steps are depicted in *Figure 25*. A channel (1,50 cm long x 200 µm wide x 20 µm high) was formed by enclosing two epoxy strips, henceforth called spacers. The spacers were made by injection moulding of Poly-Pox Injection epoxy resin plus polyamine harder in 2:1 ratio (Poly Service, Amsterdam, Netherlands) into a PDMS model device II structure that was not plasma-treated. A image of this filling process is in the Appendix *Figure 56*. This PDMS structure contained pillars to prevent the PDMS ceiling from collapsing. The epoxy resin was hardened until it was solid but still sticky (~35 min at 80 ºC). The PDMS structure was removed while the epoxy spacers remained attached to the glass (not called resin anymore). Excess spacer material near the epoxy injection site was cut away by hand. The top glass slide was pressed on top of the epoxy pacers using vices and this construct was further cured at 80 ºC (cure duration kept to a minimal when using PAA-functionalised glass).

The entry (~0.1 mL reservoir) and exit of the channel were designed with Solidworks 2015, converted with Cura 2.3.0, and printed with Ultimaker 2 3-D printer (Geldermalsen, Netherlands). These prints were attached to the bottom glass plate by 'case-II swelling' using chloroform (Haga, 1981). To prevent leakages, UV curing glue (N-vinylcaprolactam hydroxypropylmethacrylate, Bondiq®, Canada) or chloroform were used to seal the PET (polyethylene terephthalate) print (EPR InnoPET Natural 2.85 mm, Innofil3D, Emmen, The Netherlands). An 18-gauge (1.02 mm) precision tip (Nordson EFD, USA) was attached to each exit print (*Figure 24*).

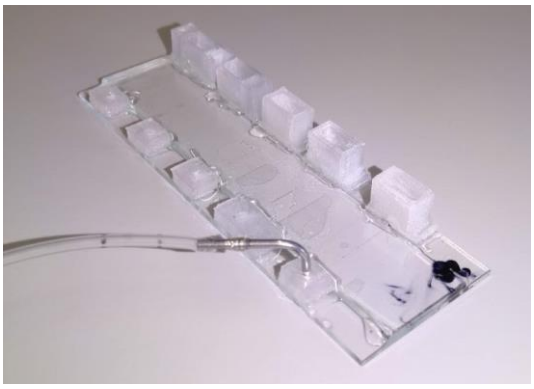

Figure 24 Photograph of five epoxy model devices on one glass slide

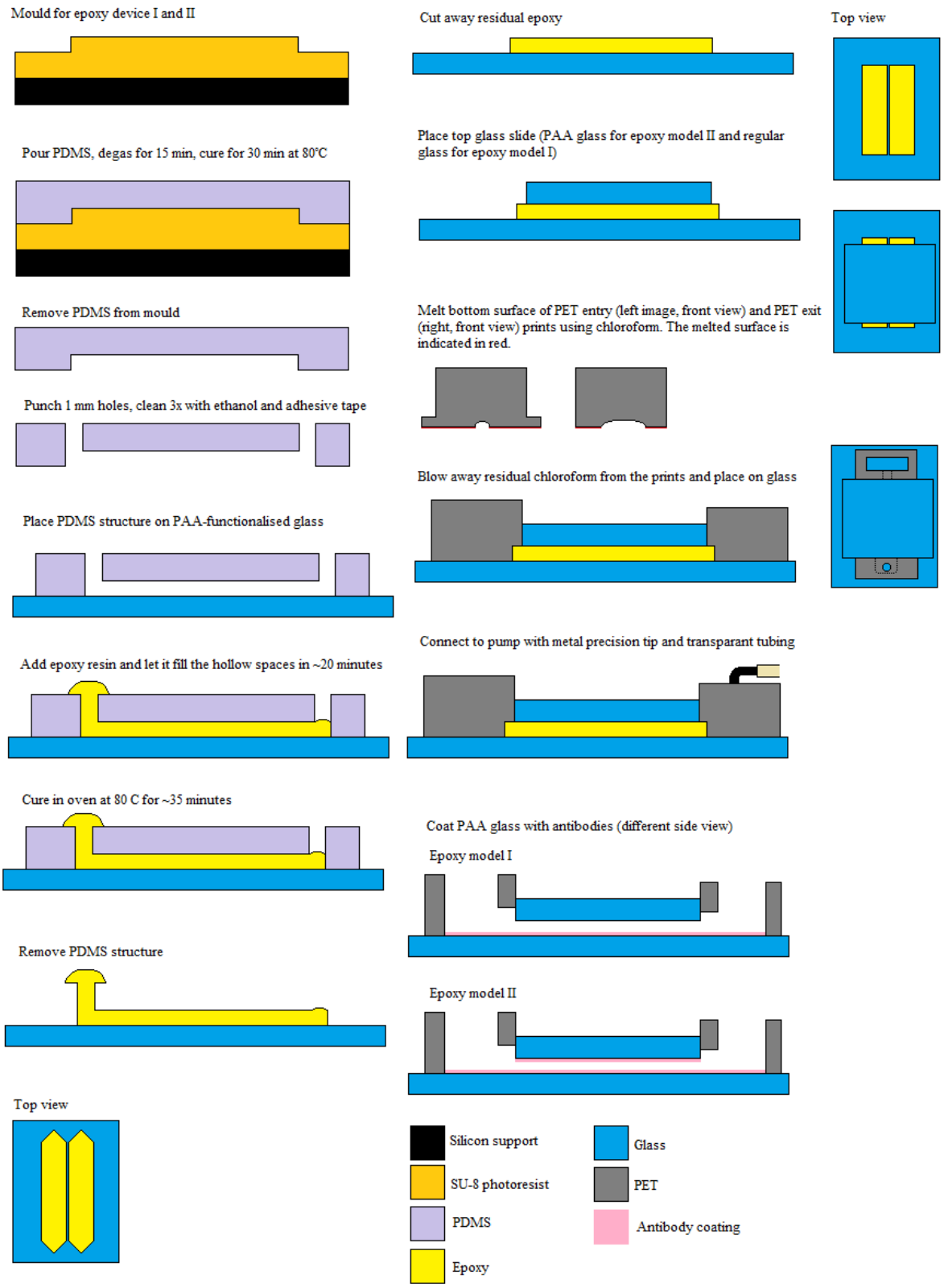

Figure 25 Schematic side-view (unless otherwise indicated) fabrication scheme for epoxy model devices III and IV. Epoxy model devices III and IV differ in the single or two-sided functionalisation with antibodies.

Vinyl spacer device

Cut vinyl stickers were cut using Silhoutte Cameo (Silhouette, Amsterdam, The Netherlands). They were placed on top of a glass slide to make spacers (*Figure 26*). The vinyl was removed, but the ~20 µm glue layer remained. The top glass slide was pressed on top of the vinyl glue spacers using vices. HF etching of glass with the vinyl spacers as resist was evaluated at 5% and 10% HF.

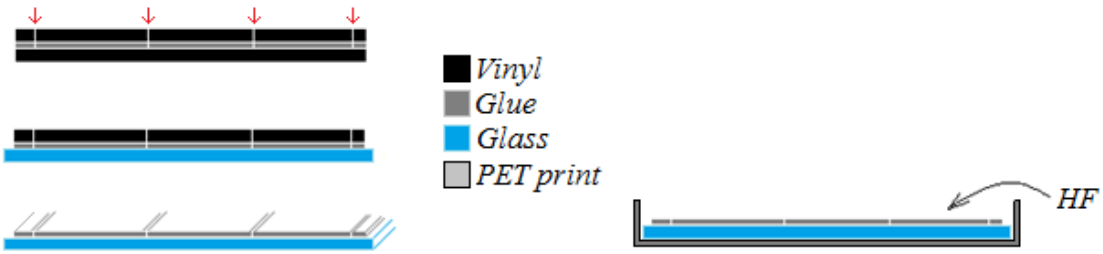

Figure 26 Vinyl spacer process, showing the cut lines with red arrows that do not penetrate the lower vinyl side. HF was poured on top of the glue spacers.

Pump and microscope

A vacuum pump (Vvap, Deventer, The Netherlands) was used to generate a negative pressure gradient. The average flow rate was determined for each experiment by measuring the travel distance of the water front in the tubing over time. The linear flow velocity in the channel was calculated for the flow rate.

Inverted microscope (Optech, UK) with illumination from top and bottom, and fluorescent microscope (Zeiss Axioskop 2 plus, Zeiss HBO 100 UV lamp with LEJ EBQ 100 Isolated power supply) with 10x10x or 10x20x magnification were used. Images were made using Moticam 2000 2.0M Pixel USB2.0 camera with Motic Images Plus 2.0 ML software, and Atik Cameras black and white camera with ArtemisCapture software. Scale bars were calibrated using Motic calibration slide.

Cell suspensions

Two human epithelial breast cancer cell lines with the same average cell size but with different epithelial adhesion molecule antigen expression levels were cultured according to guidelines from Human Nutrition group (WUR). Adherent MCF-7 and MDA-MB-231 cells were cultured in Dulbecco's modified Eagle's Medium (DMEM) supplemented with high glucose containing 1.5 $g.L^{-1}$ sodium bicarbonate ($NaHCO_3$), 15 mM HEPES buffer, 10% fetal bovine serum (FBS), and 1% of 5000 units per millilitre penicillin/streptomycin. 2 mL of 10% trypsin/EDTA (TE) solution in PBS (phosphate buffer saline solution, pH 7.4) was used for 3 minutes at 37ºC to detach cells from the surface for inoculation of new flasks with fresh medium every three to four days. The automatic cell counter at Division of Human Nutrition and Health (Wageningen, Netherlands) was used to get an indication of the cell size distribution, which varied between 18-20 µm. Blood from healthy volunteers at Division of

Human Nutrition and Health was upon collection combined with 3% (w/v) citric acid in PBS to prevent coagulation.

Antibody immobilisation on polyacrylic acid-functionalised slides

Antibody immobilisation was performed on polyacrylic acid (PAA) functionalised glass slides (Aquamarijn, Zutphen, The Netherlands). After devices were fabricated and cleaned with Milli-Q (MQ) and 0.2 µm filtered PBS, the channels were incubated for 30 minutes with a filtered solution of 1-ethyl-3-[3-dimethylaminopro-pyl] carbodiimide hydrochloride (EDC, activates carboxyl groups) and N-hydroxy-succinimide (NHS, converts carboxyl groups to amine-reactive NHS esters). EDC/NHS solution was used for crosslinking PAA chains with antibodies. Then acetic acid is flowed through the channel followed by 1:25 dilution of anti-EpCAM antibody (VU-1D9, mouse monoclonal) in PBS with 60 minutes incubation time at room temperature. Unbound antibody was washed with PBS. Ethanolamine is incubated in the channel for 30 minutes to block free PAA binding sites. (Andree et al., 2016; E. Ng et al., 2013; Ruf et al., 2007).

IgG-PE test of anti-EpCAM functionalisation: After experiments, the devices were washed with PBS and incubated with 1:20 dilution of anti-IgG-PE stock (Anti-Mouse IgG (whole molecule) F(ab′)2 fragment–R-phycoerythrin labelled antibody produced in sheep, P8547 Sigma), prepared in PBS, for 15 minutes, followed by washing with PBS. A positive signal with the Texas Red filter indicated successful antibody immobilisation. Anti-IgG-PE binds to nearly all IgG antibodies, including anti-EpCAM. Because of the bound PE label (phycoerythrin, pigment present in red microalgae), the anti-IgG-PE is visible with fluorescence microscopy.

Antigen qualification

Live cells were added to 48-wells plate according to *Table 3* and incubated overnight for cell attachment. 1:25 dilution of anti-EpCAM stock (1.1 mg.mL^{-1}) and a 1:20 dilution anti-IgG-PE stock were prepared in PBS. Spent medium from the 48-wells plate was removed by pipetting. The cells were washed twice with 200 µL 1x PBS from the refrigerator. 100 µL 1x PBS was added to all wells and 10 µL anti-EpCAM mix was added to certain wells and incubated in cold and dark for 60 minutes. The cells were washed with 200 µL PBS to remove unbound anti-EpCAM antibodies. 100 µL PBS was added to all wells and 10 µL diluted anti-IgG-PE was added to certain wells and incubated for 60 minutes in cold and dark. The cells were washed with 200 µL PBS to remove unbound IgG-PE antibodies. (Nima et al., 2014)

Table 3 Scheme for antigen qualification. The numbers indicate the number of live cells added per well on day one.

	1. EpCAM+/ IgG-PE+	**2.** EpCAM-/ IgG-PE+	**3.** EpCAM-/ IgG-PE-
A. MCF-7	10^4	10^4	10^4
B. MDA-MB-231	10^4	10^4	10^4
C. Medium only	200 µL	200 µL	200 µL

Data analysis

Cells were counted with icy 1.9.4.1 open source image analysis software with Manual Counting and Spot Detector plugins (F. de Chaumont, 2014). Colour replacement of fluorescent images was done with IrfranView 4.51 followed by 1:1 merge with bright field images. Calculations and statistical analysis (two-tailed *t*-Test) were done with Microsoft Excel 2016.

The recovery is defined as the percentage of captured cells within the channel relative to the total number of cells that have entered the channel. Cells that are stuck inside the reservoir are ignored. The purity is the percentage of bound circulating tumour cells compared to bound non-target cells such as red blood cells (RBCs) and leukocytes (WBCs). Release efficiency is the percentage of captured CTCs that can be released after binding, relative to the cells that remain bound. Rolling cells are not considered detached cells. Note that cells rarely attach after detaching, because the capture condition are much milder compared to the detachment conditions. The number of detached cells is equal to the number of cells that elute from the channel.

$$Recovery = \frac{\#CTCs\ captured}{\#CTCs\ that\ entered\ the\ channel} * 100\%$$

$$Purity = \frac{\#CTCs\ captured}{\#CTCs\ captured + \#WBCs + \#RBCs} * 100\%$$

$$Release\ effiency = \frac{\#CTCs\ detached}{\#CTCs\ initially\ captured} * 100\%$$

Results and discussion

Antigen qualification

As this thesis is based on the selective capturing of MCF-7 cells based on their overexpression of EpCAM antigen and the near-absence of this antigen on MDA-MB-231 cells, the presence of these antigens was verified. Anti-EpCAM antibodies that bind with EpCAM antigen on a cell's surface were added to cell suspensions. Next, anti-IgG-PE that binds to the anti-EpCAM antibodies was added and unbound molecules were washed away. *Figure 27-A* shows that MCF-7 were able to bind anti-IgG-PE, indicating the presence of EpCAM antigens. All controls, including MDA-MB-231 cells, gave no clear signal under the fluorescence microscope (*Table 4, Figure 27-B, C, Figure 28-A-C)*, indicating the absence of EpCAM antigens on the surface of MDA-MB-231 cells. From this experiment it was concluded that the chosen cell lines MCF-7 and MDA-MB-231 were suitable as positive and negative control respectively.

Table 4 Results of EpCAM antigen qualification using PE labelled IgG and anti-EpCAM.

Cell line	Cells + Anti-EpCAM + IgG-PE	Cells + IgG-PE	Cells
MCF-7	+	-	-
MDA-MB-231	-	-	-

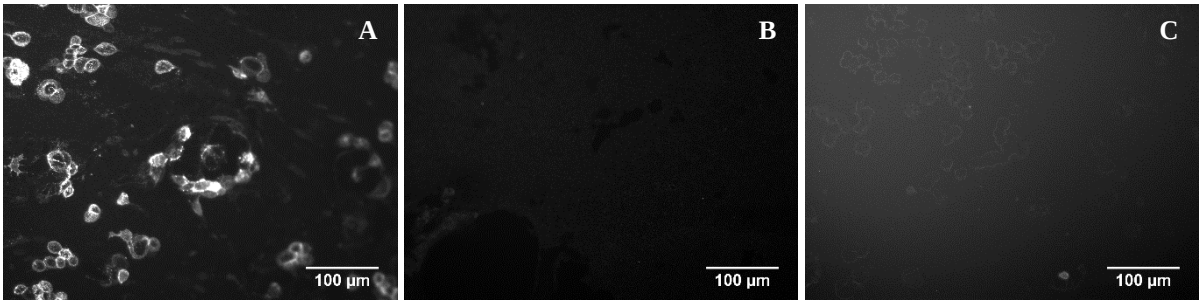

Figure 27 Fluorescent images of MCF-7 cells at 10x magnification, 1 second camera exposure. A) Anti-EpCAM + anti-IgG-PE. B) Anti-IgG-PE. C) Only cells. The scale bars are 100 µm.

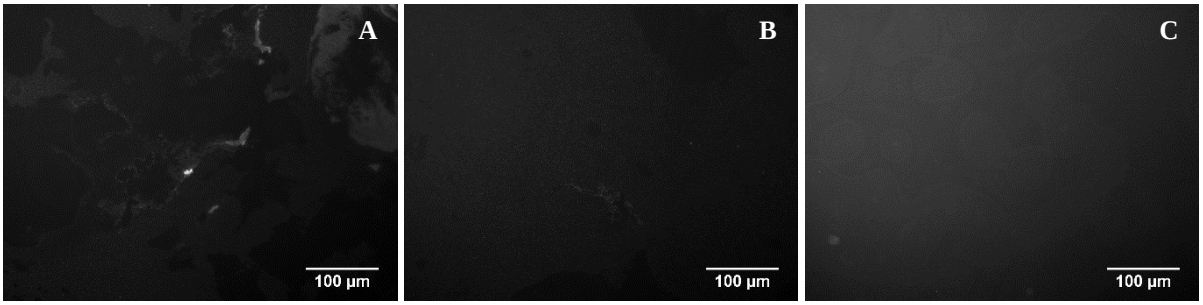

Figure 28 Fluorescent images of MDA-MB-231 cells at 10x magnification, 1 second camera exposure. A) Anti-EpCAM + anti-IgG-PE. B) Anti-IgG-PE. C) Only cells. The scale bars are 100 µm.

Antibody immobilisation test

The presence of antigens was verified. These antigens bind to the antibodies that were coated in the inner surface of the channel for affinity-based cell capturing. Antibody immobilisation success was verified using anti-IgG-PE test. Anti-IgG-PE binds to and identifies the presence of anti-EpCAM antibodies (*Figure 29*).

Figure 30 shows verification of the procedure: antibody functionalisation was only successful in the presence of EDC/NHS to crosslink the antibodies with the PAA chains on the glass surface.

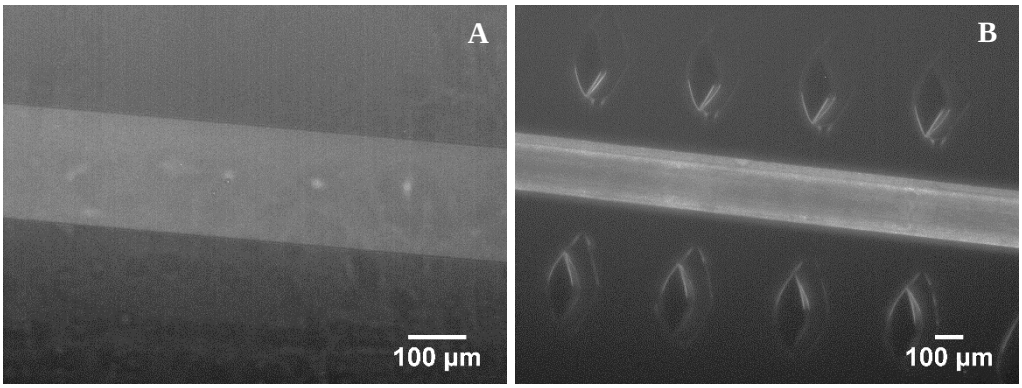

Figure 29 Antibody coating verification after cell experiments. Fluorescent images of (A) the epoxy channel at 20x magnification and (B) the PDMS channel at 10x magnification.

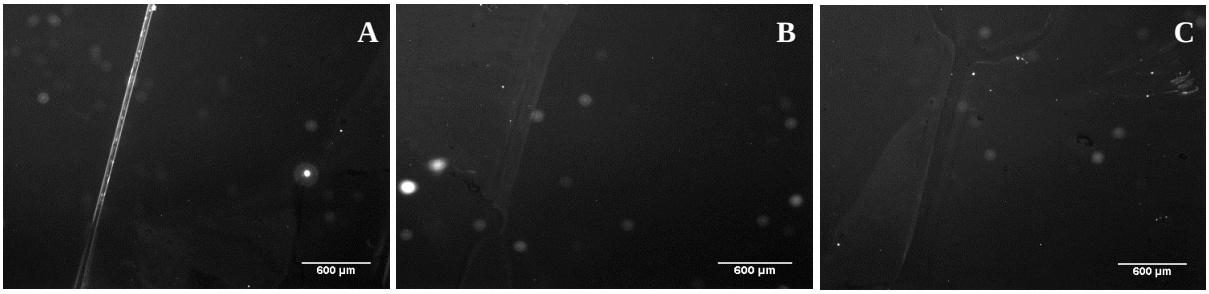

Figure 30 Antibody coating procedure verification showing PDMS device model I channels at 5x magnification. (A) EDC/NHS ''linker'' plus anti-EpCAM antibodies, positive signal expected. (B) No linker, only anti-EpCAM antibodies, negative signal expected. (C) EDC/NHS linker without anti-EpCAM antibodies, negative signal expected

Anti-biofouling of polyacrylic acid-functionalised glass slides

The complex formation of EpCAM antigen and anti-EpCAM antibodies is specific. Non-specific binding of blood cell (biofouling) was evaluated. It was observed that red blood cells (RBCs) stuck to regular glass slides (*Figure 31-A*). They also remained attached during washing with PBS up to a linear flow velocity of 13.2 mm.sec^{-1} (a flow rate of 0.317 mL.min^{-1}) (*Figure 31-B*). As predicted, RBCs did not stick to PAA-functionalised glass slides (without antibody coating). *Figure 32-A* shows RBCs flowing through the channel, and *Figure 32-B* shows that no cells were attached. In both cases, pure blood was used. An explanation for these results is the hydrophilicity of the PAA chains: a water layer forms between the glass surface and the RBC within and near the PAA coating, which prevents the RBC from attaching to the glass.

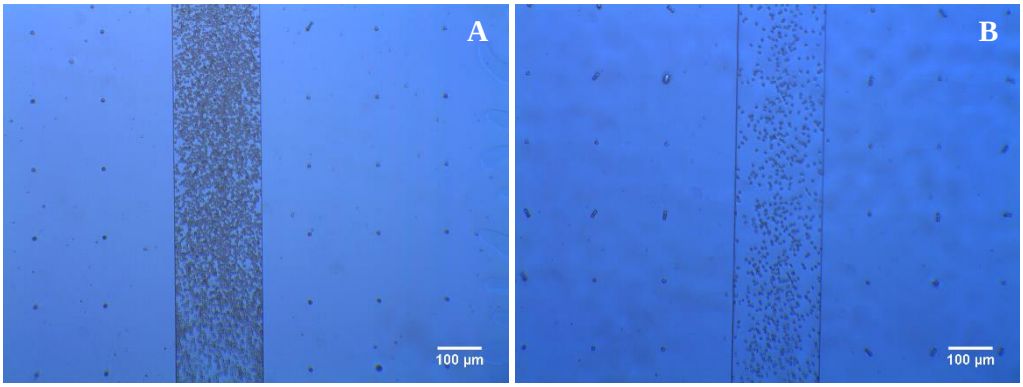

Figure 31 (A) Red blood cells stick to the regular glass slides, and (B) stay attached during washing with 13.2 mm.sec^{-1} (0.317 mL.min^{-1}).

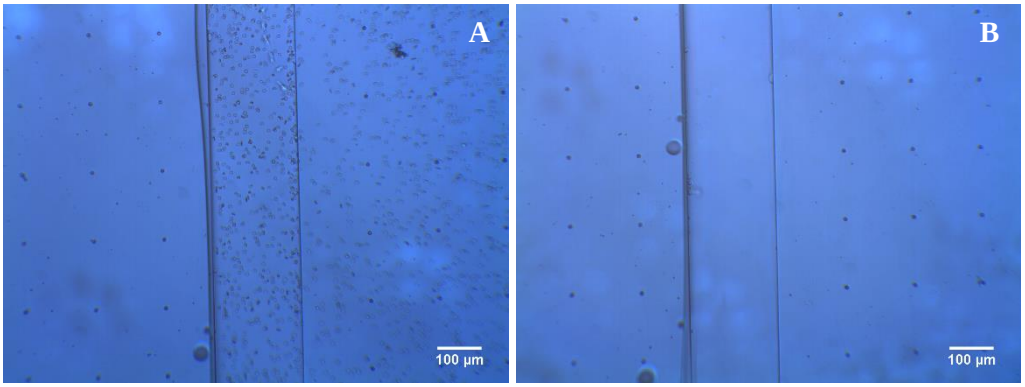

Figure 32 (A) Red blood cells flowing through the channel, note that these are not bound to the surface. These small cells (6-8 µm) could also find their way into the gap between epoxy spacer and the top glass slide. (B) No cells remained present after washing at 8.1 mm.sec^{-1} (0.194 mL.min^{-1}).

Evaluation of device fabrication

Device fabrication

Using an inverted microscope, the starting line of the channel could easily be found for the devices made from vinyl spacers and from epoxy spacers (*Figure 33*). The glass edge formed the entry of the channel, so the start line was well-defined. The PDMS device, however, did not have a well-defined starting line because it was curved and microstructures from the mould were still partially present.

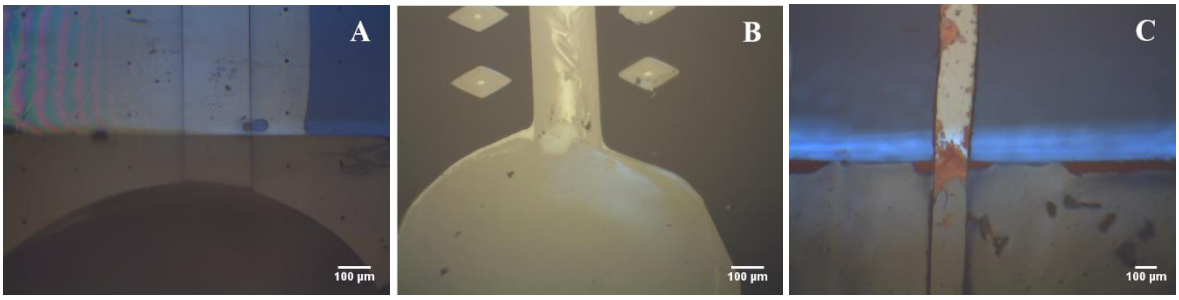

Figure 33 Starting lines of the channel from different devices, with the reservoir in the bottom half of the images. (A) Epoxy spacer device with fluid (dark circle) filling the reservoir and nearing the channel entry, (B) empty PDMS device, not clearly showing presence of microstructures, and (C) used vinyl glue device.

Cell quantification was facilitated by the horizontal channel orientation relative to the microscope objective. Also, glue that was used to seal the entry and exit prints for an air-tight seal with the glass slides did not inhibit cell observation, because an inverted microscope was used.

Adams et al. reported consistent device failure at a channel height of 20 µm due to entry blockage and cover plate detachment. Device failure due to entry blockage occurred three time for the vinyl glue device and two times in the PDMS channel, of which the latter occurred not by cells but by large debris or dust. Top glass plate detachment was never observed.

For fabrication of epoxy devices, PDMS pillars were attached to the PDMS mould ceiling to prevent the ceiling from collapsing, which would be driven by the surface tension of entering epoxy resin. These pillars were too short due to a fabrication complication, so they did not reach the bottom glass plate, rendering them ineffective (*Figure 34* shows too short pillars). This yielded uneven epoxy spacers which allowed fluid and small cells to enter the gap between the top of the epoxy spacer and the bottom of the top glass slide. Newton rings were visible, indicating a height difference between the spacer and the top glass slide (*Figure 57* in the Appendix). Due to this fabrication issue, a limited data set on cell capturing dynamics was obtained. Improved devices could be fabricated by employing a more robust pillar design or improved mould fabrication precision.

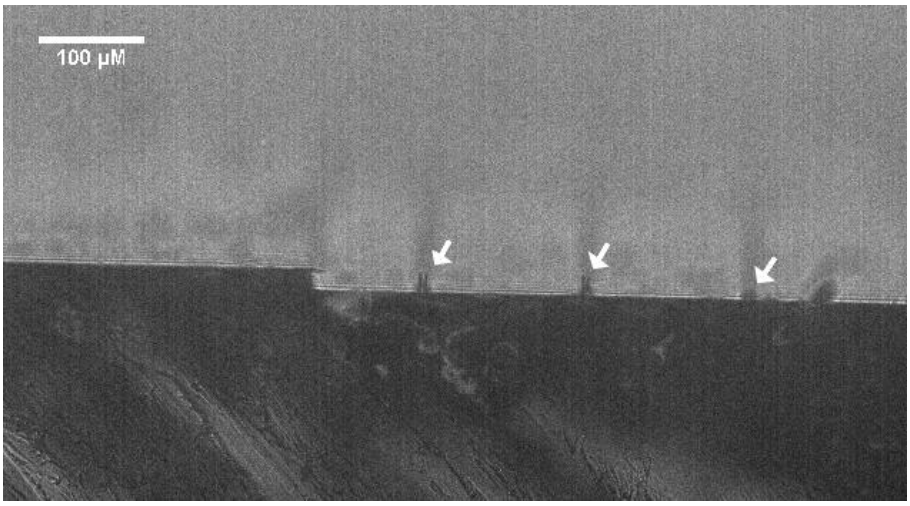

Figure 34 Cross section of the PDMS model device II (dark area) placed upside down, exposed to air. The PDMS device model II was the mould for epoxy resin for epoxy model devices III and IV. The pillars (indicated with arrows) were insufficient in length and possibly rigidity to prevent the PDMS ceiling from collapsing. The noise above the arrows are out-of-focus pillars.

The result of this 'pillar problem' can be seen in the next two images in which red blood cells (6-8 µm, *Figure 35*) and in some cases even circulating tumour cells and presumed white blood cells (20 µm, *Figure 36*) were able to migrate over the spacers.

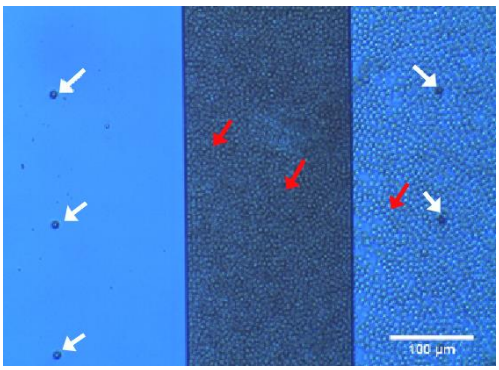

Figure 35 Top views of an epoxy device model. Small red blood cells (red arrows) creeped into the space between the epoxy spacer and the top glass slide on the right side of the image. The spacer of the left side was fully bonded with the top glass slide. All pillar are indicated with white arrows.

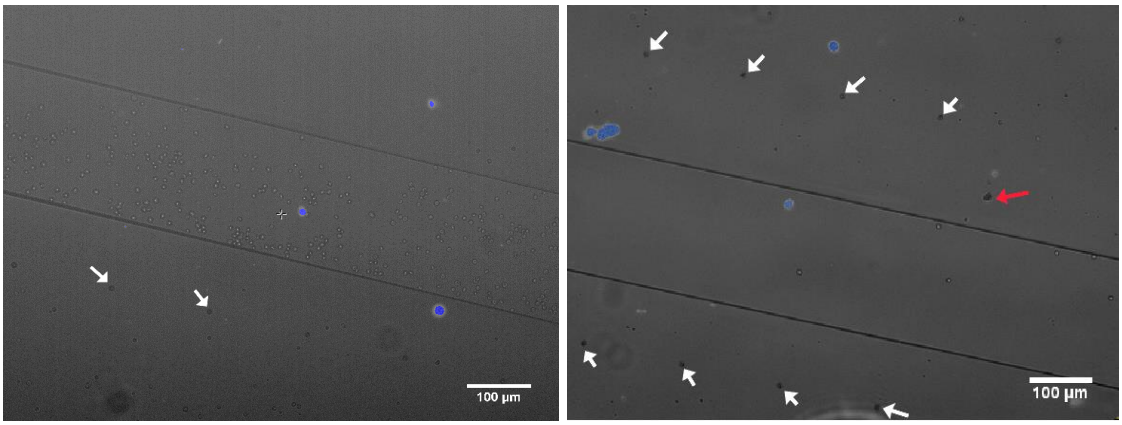

Figure 36 Epoxy device models III showing red blood cells (RBCs) and acridine orange-stained MCF-7 cell (blue) inside the channel. Outside of the channel, two MCF-7 cells are retained. All RBCs that were present outside of the channel were washed out using PBS, while the large MCF-7 cells are physically stuck. Two pillars are indicated with arrows and likely a white blood cell is indicated with a red arrow.

A delay of maximally one second was observed for cell movement inside all channels after shutting down the vacuum pump. Because of this rapid change of cell velocity, it is possible to operate the devices in a stop-and-go manner (not done in this thesis). This aids cell capture because cells are given the time to bind to the coating, but the overall flow rate decreases.

The maximum height of the semi-circular PDMS model device I was measured at 32.8 µm and the height of the other devices 20.1 µm.

The fabrication of the vinyl glue devices was not successful, because the channels were not smooth (straight) and their width was not constant (*Figure 37* shows channel deformations). Gas was able to diffuse into the channel when operating at large pressure gradients.

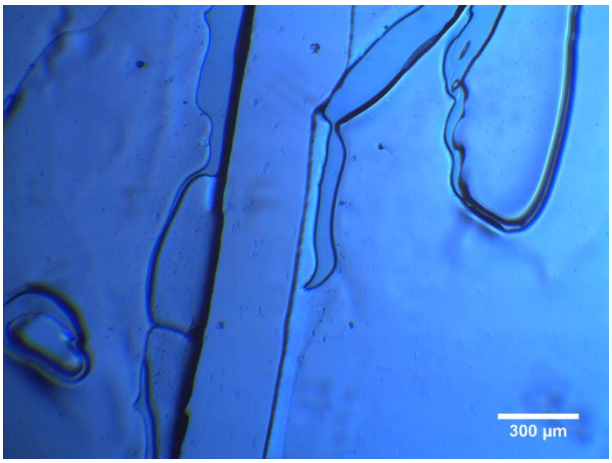

Figure 37 Vinyl glue device having non-uniform channel width (wider channel at the top of the picture) and gas pockets between the glue and the top glass slide.

Evaluation of device performance

Table 5 summarises the performance of the model devices of this thesis compared to similar devices reported in literature. The linear flow velocity and throughput were achieved at the mentioned recovery. It was not possible to accurately estimate the recovery of PDMS model device I. As a frame of reference: the flow velocity in a medium-sized blood vessel is 10-50 mm.sec^{-1} (Theil et al., 2016).

Table 5 Overview of the analysed devices compared to devices described in literature. [A]: Larger flow velocities were not yet tested. [B]: The time required for sample processing and assay preparation (B. Hong & Zu, 2013). [C]: compare with all models. [D]: compare with epoxy model devices III & IV. [E]: compare with PDMS model device II. [F]: Discussed earlier in this report. NM: Not mentioned. NA: Not applicable.

Assay	**Sample volume**	**Recovery η belonging to V**	**Linear velocity *V* (mm.sec^{-1})**	**Throughput per channel (mL.min^{-1})**	**Limitations**
		η at maximum V	**Maximum *V***		
PDMS model I	Unlimited	NA	37.3	0.317	Operation not optimised, weaker binding due to a 30 µm channel height, allowing the larger cells to detach.
PDMS model II micro-post array	Unlimited	98%	0.1[A]	0.026[A]	Stagnant areas with non-specific binding.
Epoxy model I	Unlimited	25%	5.6[A]	0.134[A]	Fabrication and operation not optimised.
Epoxy model II	Unlimited	95%	5.3	0.128	Fabrication and operation not optimised.
		~50%	*18.7*	0.449	
CTC-Trap[C]	Unlimited	30-60%	0.4	0.005	Non-specific binding in stagnant areas.
			0.7		
HTMSU[D]	Unlimited	97%	2	0.005	Tested for 1 mL as 'large sample volume', no negative control.
		40%	10		
CTC-Chip micro-post array[E]	3 mL	65%	NM	0.033	Limited sample volume.
CellCollector™	Unlimited	10-35%	10.2	5.1	Low recovery, long time required for enumeration.
CellSearch®	7.5 mL	40-82%[F]	NA	90 minutes[B]	Limited sample volume.
ISET	10 mL	NM	NA	142 minutes[B]	Limited sample volume, missing small CTCs, low purity.

Cell distribution

Before results with the device models are discussed separately, the results of cell distribution experiments are shown. The goal of this thesis was to test the possibly of capturing CTCs within a pore of 1 mm in depth. In the HMTSU and CTC-Trap, most captured cells were captured in the first 1-2 mm and of the 3.5 mm and 5.2 mm long channels, respectively. In the epoxy devices and PDMS device model I, with a few exceptions in the beginning of this thesis, all captured cells were found in the first millimetre of the channel. This result is very promising for a microsieve with a maximum channel length of 1 mm. By pooling cell capture data of multiple flow velocities, *Figure 38* was obtained. These diagrams both show that if a cell is captured, it is likely it will be captured in the first 400 µm of the channel. The likeliness of finding captured cells decreases with increasing distance from the channel start line. These findings are relevant for the microsieve device design: the data imply that the performance of the microsieve will not drastically increase with increasing pore depth above the proposed 1 mm pore depth.

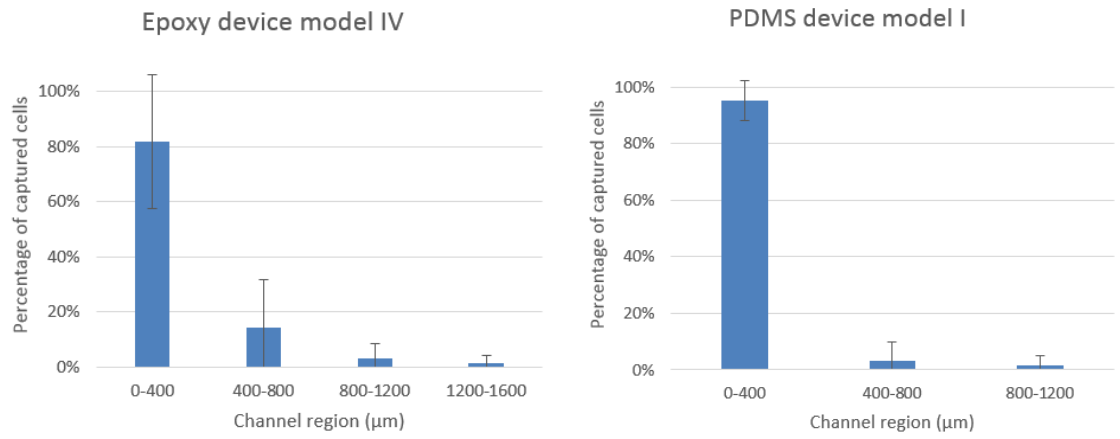

Figure 38 Cell distribution of MCF-7 cells in the epoxy device model IV (left) and the PDMS device model I (right). Cell capture data from one device with multiple flow rates were pooled.

The next step was finding the relation between linear flow velocity and cell attachment region. Goldsteen proposed that the capture length $L_C \approx e^V$. L_C is defined as the length from the channel start at which 63% of the cells are captured. As stated in Goldsteen's report, a channel operated at 1 mm.sec^{-1} would require a length of 4.8 meter to capture 63% of the entered cells. This model does not hold up specifically for the devices evaluated in this thesis. Unfortunately, no alternative model for the attachment region could be proposed by plotting cell capture data from this thesis as a function of average linear flow velocity, (*Figure 38*). It was expected that the percentage of captured cells would decrease with increasing flow velocity.

According to the data, *if* a cell is captured, they are captured near the entry, and the attachment location is not a function of flow velocity. Going back to the theoretical background: a faster relative flow velocity results in a decreased binding rate (Chang & Hammer, 1999), with the binding rate being the number of formed antigen-antibody complexes per unit of time. Therefore, relative flow velocity (the velocity of the antigens relative to the stagnant antibodies) determines the total number of complexes the cell can initiate with the antibody-coated surface per unit time, at each moment in time. The number of formed complexes per unit time (binding rate) does not change in time because the relative velocity does not change over the channel length. The binding rate is constant over the full channel length; binding rate and channel length are not linked. This could explain why no relation between flow velocity and cell distribution was found.

The reason why some cells are captured, while other cells are never captured, can be given by adding biological variables to the above relation of flow velocity with binding rate.

(1) Cells are not all equal in size;
(2) the antigen concentration might not be equal for every cell;
(3) the total number of antigen on the cells' surface is not equal for every cell.

The number of antigen-antibody complexes the cell can initiate at a certain moment in time is dependent on the number of antigens that the cell presents to the antibody coating. Now image, depending on the cell's size (relates to drag force), a cell requires X number of antigen-antibody complexes to be captured (relates to total binding strength). The relative flow velocity and the number of antigen the cell represents to the antibody coating at a certain moment in time combined yield a binding rate of Y complexes per unit time. Logically, the cell would require X/ Y time to be captured. However, after time Z has passed, the cell has already moved forward in the channel and thereby dissociated the first few formed complexes, i.e. X will never be reached when $Y < X$. This explains why some cells (low required X by a small cell size or high Y by many presented antigens per unit time) are captured while other are cells (high required X by a large cell size or low Y by few presented antigens per unit time) are never captured at a specific flow rate.

So when a cell has favourable number of antigens (which determines binding strength) relative to its size (which determines drag force), it will be captured in the channel, and the place of cell attachment is near the channel entry. When a cell have less favourable number of antigens relative to its size, the cell will not be captured in the channel. Increasing the channel length does not increase the change for each cell to be captured eventually. This means that for a specific channel geometry and operating conditions, upon the moment a cell enters the channel, this cell does not have a binding chance anywhere between 0 and 100%, but either 0% of 100%. If this chance of 0%, it will not be captured (not near the

entry and not near the exit). It this chance if 100%, the cell will be captured somewhere near the entry of the channel.

A reason why a cell would randomly attach to the coating, would be non-homogeneous distribution of antigens over the surface: at a certain moment, the number of antigens presented by the cell in the right direction (to the antibody-coated surface) favourable enough for cell capture. Random distribution over the channel was not observed, and this hypothesis is also theoretically unlikely because of the many thousands of antigens per cell that can homogeneously distribute over the fluid-like plasma membrane (Singer, 1972).

Based on the current data set, no clear relation between flow velocity and capture region could be defined (*Figure 39*).

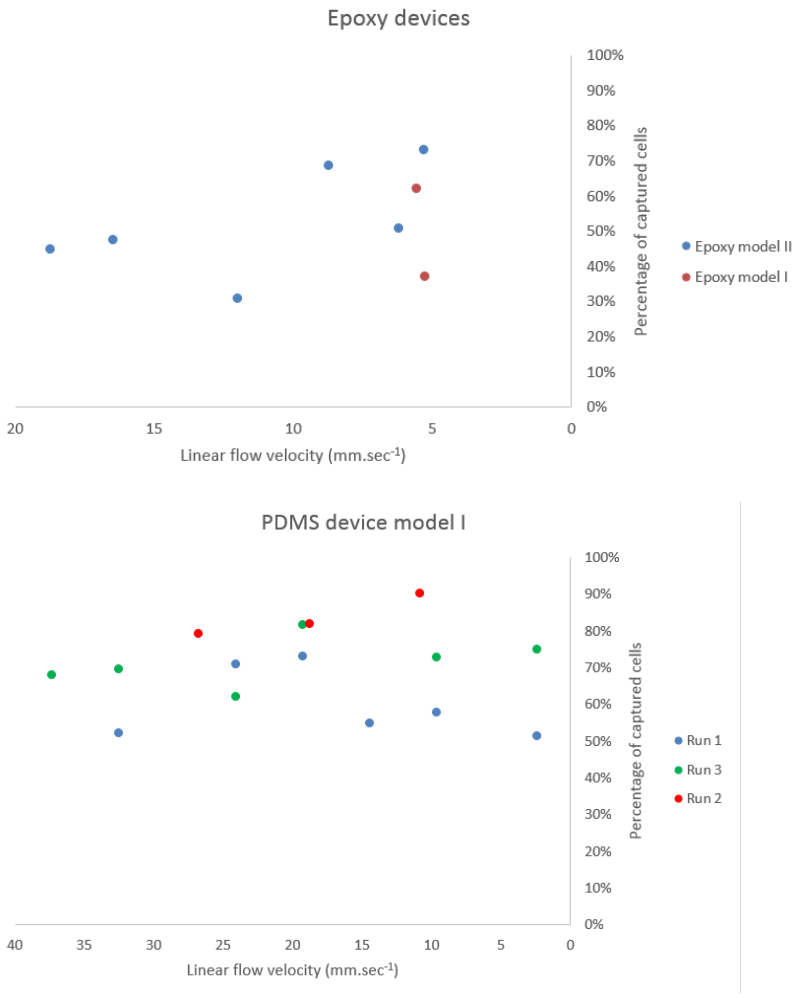

Figure 39 Percentage of captured cells in the first 200 µm of the channel as a function of linear flow velocity in epoxy model devices (top figure) and PDMS device model I (bottom figure). One outlier in the epoxy data set was deleted because of unreliable flow velocity value. These data can be seen as the likeliness of finding all captured cell in the first 200 µm of the channel.

Cell capture using PDMS model device I

PDMS device model I captured 354 MCF-7 cells in culture medium at an average linear flow velocity in the channel of 13.2 mm.sec^{-1} (0.112 mL.min^{-1}), 20% of the captured cells were captured in the first millimetre of the channel. 93% of the cells remained attached after washing with PBS at 20.6 mm.sec^{-1} (0.175 mL.min^{-1}). In another run, 65% of the cells remained attached after washing with PBS at 30.1 mm.sec^{-1} (0.252 mL.min^{-1}). An image of cell capture plus the cell enumeration is shown in *Figure 42*.

Cells started to attached at an average (n = 3) average linear flow velocity of 32.2 mm.sec^{-1}, with low recovery. The number of captured cell after one minute of running at specific velocities was determined (cell capture rate), resulting in *Figure 40*. Assuming equal number of cells entered the channel in each experiment, a clear trend is visible: the recovery increases with decreasing flow velocity.

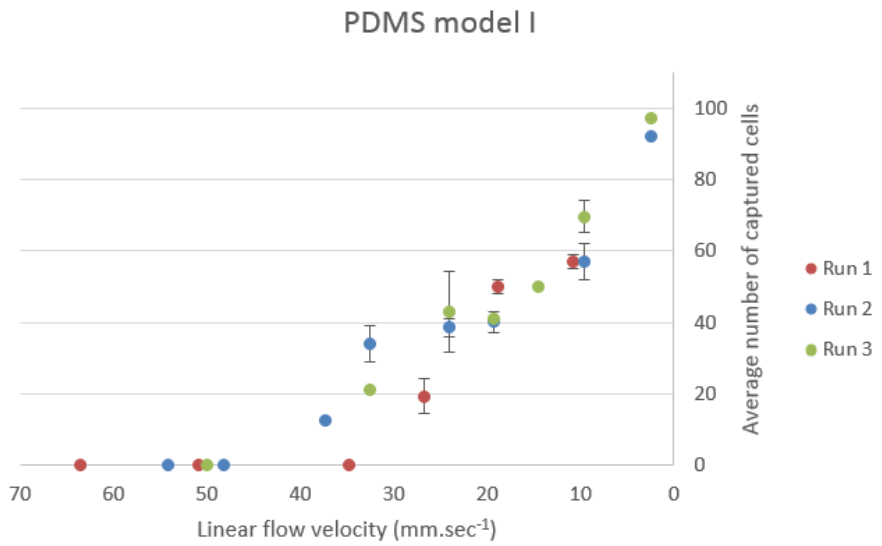

Figure 40 MCF-7 cell capture numbers from three experiments. The channel was emptied before a new run was started. Each velocity was tested twice for 1 minute per run, using the same cell concentration in the reservoir. The linear flow velocity values were interpolated based on flow rate data.

In a run with MCF-7 cells spiked in whole blood, MCF-7 cells were captured at 9.1 mm.sec^{-1} (0.077 mL.min^{-1}) and remained bound during washing with PBS at 11.8 mm.sec^{-1} (0.100 mL.min^{-1}). After washing, ~99% of present red blood cells were washed off while MCF-7 cells were retained (*Figure 41*). WBCs were not pre-stained, so the purity cannot be assessed accurately. Also, calculating the recovery was not possible because not all the non-captured cells remained in the exit reservoir, because the flow velocity was too high for sedimentation (this was not the case for the epoxy device models).

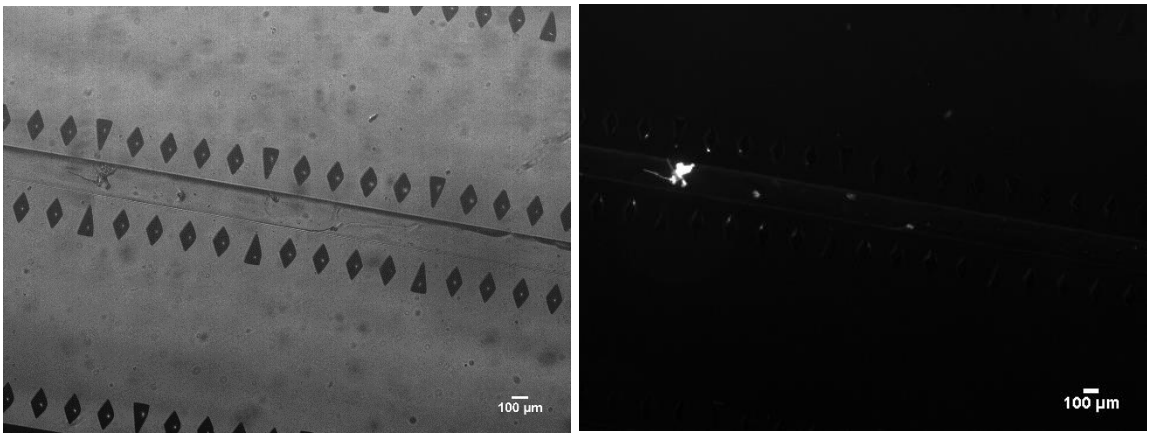

Figure 41 (A) Bright field image of PDMS model device I channel with captured MCF-7 cells. (B) Shows the same channel area with fluorescence microscopy using the Texas Red filter (emission only between 630 and 669 nm). The MCF-7 cells were pre-stained with acridine orange, which is a fluorescent label for DNA (excitation at 502 nm, emission maximum at 525 nm) and RNA (excitation at 460 nm and emission maximum at 650 nm).

39 MDA-MB-231 cells were captured at 12.02 mm.sec^{-1} (0.102 mL.min^{-1}), but no cells remained attached after washing with the same conditions at which 93% of the MCF-7 cells remained attached (PBS, 20.6 mm.sec^{-1}, 0.177 mL.min^{-1}). This was repeated: 10 MDA-MB-231 cells (<<1% recovery, 50% in first 1 mm) were captured, but no cells remained attached washing at low velocity. When using atmospheric air pressure to flow, a 0.3 mm.sec^{-1} cell velocity was achieved (calculated from a video recording). At this low velocity, 12% of the passing MDA-MB-231 cells attached, of which no cells remained attached after re-starting the pump at its smallest pressure gradient (5 mBar, ~5 mm.sec^{-1} fluid flow velocity inside the channel). The cells that were 'captured' were either sedimented or experienced physical resistance in the narrow channel.

Because channels that were not coated with anti-EpCAM did not show any cell capture and because no MDA-MB-231 cells remained attached after mild washing, it was concluded that the MCF-7 cells were captured based on antigen-antibody complex formation.

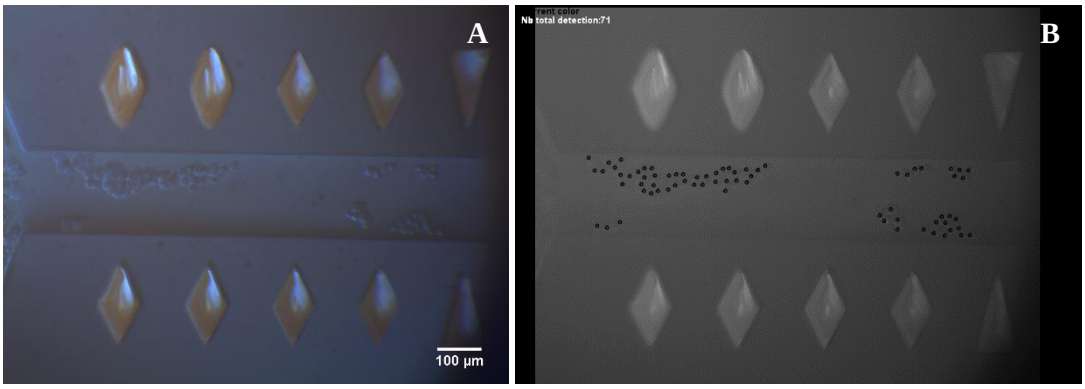

Figure 42 MCF-7 cells captured in the PDMS model device I entry region (first 1 mm). (A) Bright field image of the captured cells, and (B) showing the digital enumeration of image (A), with each black dot as a count incidence.

Cell capture using PDMS model device II

The PDMS model device II was similar to the CTC-Chip (also a micro-post array), and was similar in dimension the CTC-Trap. It was calculated that a recovery of 98% of MCF-7 cells was achieved at an average linear flow velocity of 0.1 mm.sec^{-1}; a flow rate of 0.026 mL.min^{-1}. *Figure 45* shows many cells at the entry and few cells at the exit. The micro-posts aided MCF-7 cell capture (*Figure 46*).

About 40% of the attached cells detached from the surface by increasing the average flow rate to 0.204 mL.min^{-1}, and another ~40% detached using 1.71 M NaCl at the same flow rate (*Figure 43-A-C*). The flow velocity was not homogeneous in this device, so attach and detach linear flow velocities in the channel are unreliable. In some areas, the cells did not detach because washing fluid was not reaching the cells in these stagnant areas.

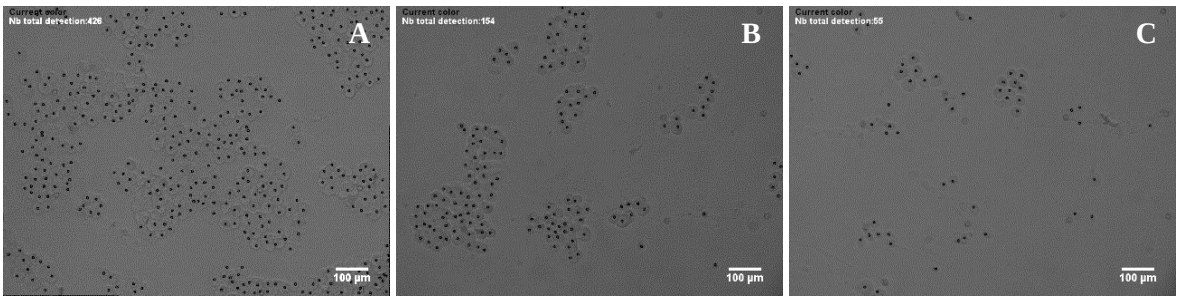

Figure 43 Enumeration of MCF-7 cells in 2nd mm of the PDMS model device II. (A) Before washing, (B) after washing with PBS, (C) after washing with 1.71 M NaCl. The black dots are count incidents. Cell debris is also visible.

Stagnant areas were expected to arise in this channel: laminar flow (Re <1) and no-slip boundary condition result in a parabolic flow profile with slow velocity near the sides of the channel, which increases the deposition of cells here, which inhibits free fluid flow here. This is also the case for the narrow PDMS channel, but the flow velocity that a cell near the sides experiences is different for the two channels. To simplify, assume the velocity profile is linear of the width of the channel (*Figure 44*). This yields the following formula for the velocity difference ΔV over the cell surface[1]:

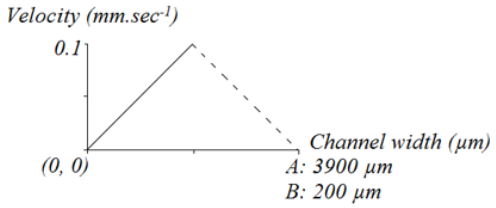

$$\Delta V\left(\frac{mm}{sec}\right) = \frac{Maximum\ velocity\ \left(\frac{mm}{sec}\right)}{Half\ channel\ width\ (\mu m)} \cdot cell\ diameter\ (\mu m)$$

Figure 44 Simplified velocity profile over the channel with a maximum velocity of 0.1 mm.sec^{-1} and no flow at the sides of the channel (no-slip condition).

[1] This formula holds up for half of the channel.

Using this formula, the *average* flow velocity over the cell surface when it is attached to either side of the channel is 0.25 µm.sec^{-1} for the wide channel and 5 µm.sec^{-1} for the narrow channel (other velocities shown in *Table 6*). This difference explains the increased cell sedimentation in the wide channel compared to the narrow channel.

Table 6 Comparison of linear flow velocities over the cell surface in PDMS model device I (200 µm) and II (3900 µm). [A]: per definition according to no-slip boundary condition.

Total channel width	**Position of the cell**	**V on the left side of the cell (mm.sec^{-1})**	**V on the right side of the cell (mm.sec^{-1})**
3900 µm	Left side of the channel	0 [A]	0.0005
3900 µm	Middle of the channel	0.0997	0.997
200 µm	Left side of the channel	0 [A]	0.01
200 µm	Middle of the channel	0.095	0.095

MDA-MB-231 cells (negative control) were also captured in the stagnant areas of the wide channel (*Figure 47-A*), followed by the formation of narrow streamlines in the centre via which newly entered cells quickly flowed from entry to the exit (*Figure 47-B*). The deposition in the stagnant areas was more random compared to MCF-7 cells: the MDA-MB-231 cells were less likely to attach near a micro-post. From this it can be concluded that MCF-7 cells attach to the anti-EpCAM antibodies once their velocity is locally decreased by the obstruction of a micro-post, while MDA-MB-231 cells randomly sediment.

The large width caused unspecific cell sedimentation which could not easily be washed away, as the washing fluid travels along the formed centre streamlines ('highways'). The purposeful formation of highways was described by Goldsteen (2016), with the goal of having regions with low cell velocity for cell binding and a high overall volumetric throughput. Here it was found that these highways cause non-homogeneous flow velocity and unspecific cell binding in the low velocity areas.

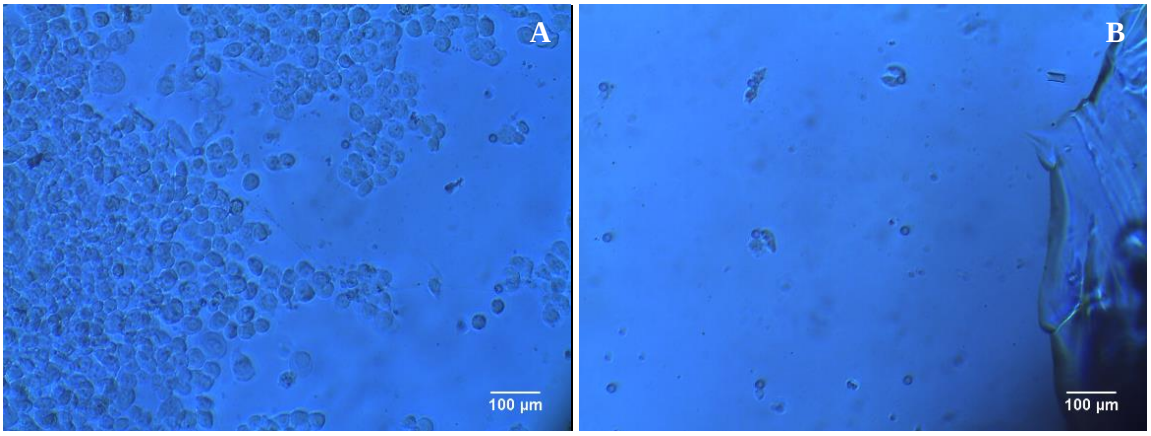

Figure 45 Images near the (A) entry and the (B) exit, indicating MCF-7 capture with high recovery.

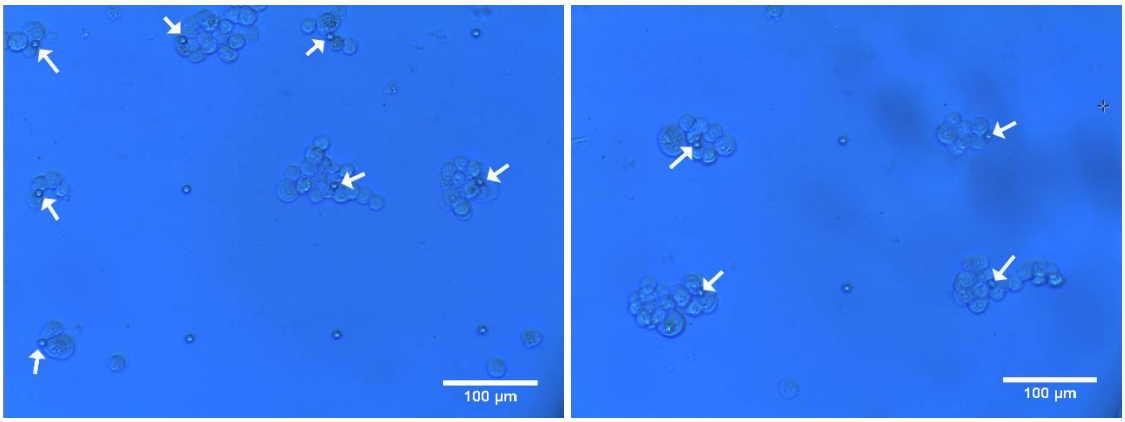

Figure 46 Two bright field images of nearly all captured MCF-7 cells attach near a micro-post. The white arrows point to micro-posts near which MCF-7 cells were captured.

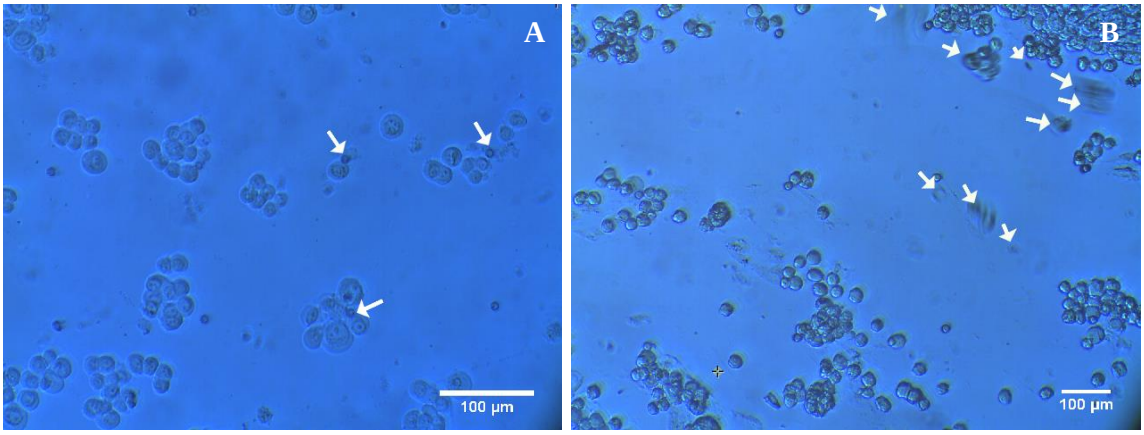

Figure 47 (A) MCF-7 cells after washing with NaCl have a decreased tendency to attach near a micro-post, i.e. the cells are sedimented instead of attached. B) MDA-MB-231 cells in the micro-post array PDMS model device II. Stagnant areas with sedimenting cells and formation of streamlines with high flow velocity without cell binding via which the cells travel to the exit. The arrows indicate moving cells via the streamlines in between sedimented cells.

To conclude: PDMS model II achieved near-perfect capture efficiency, but this was accompanied by non-specific binding of control cells because of the formation of stagnant areas and difficulty of eluting captured cells after enumeration. The micro-posts showed to be beneficial in cell capturing process, because nearly all captured cells were attached to or near a micro-post.

Cell capture using epoxy model I and II

Using the same approach as with PDMS device model I, a relation between linear flow velocity and cell capture rate was found in epoxy device model IV: decreasing flow velocity results in increasing cell recovery, or increased binding rate (*Figure 48*). The cells started to attach at a linear flow velocity of 18.7 mm.sec^{-1}, which is lower compared to the PDMS device. Due to the low aspect ratio, the flow rate of 0.449 mL.min^{-1} (sample throughput) was larger than the PDMS device, because of the low aspect ratio. The recovery of acridine orange stained MCF-7 cells (*Figure 49*) in the epoxy model II device was 95% at an average linear flow velocity of 5.3 mm.sec^{-1} (0.128 mL.min^{-1}).

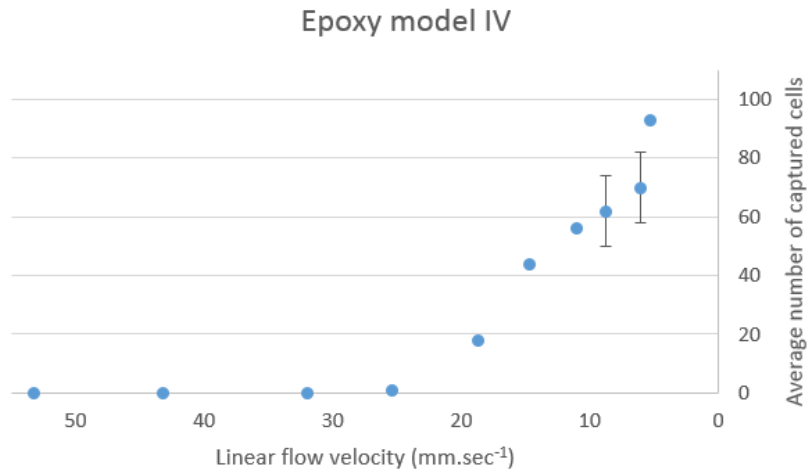

Figure 48 MCF-7 cell capture as a function of linear flow velocity. Data points with error bars are from two or more measurements at the same velocity.

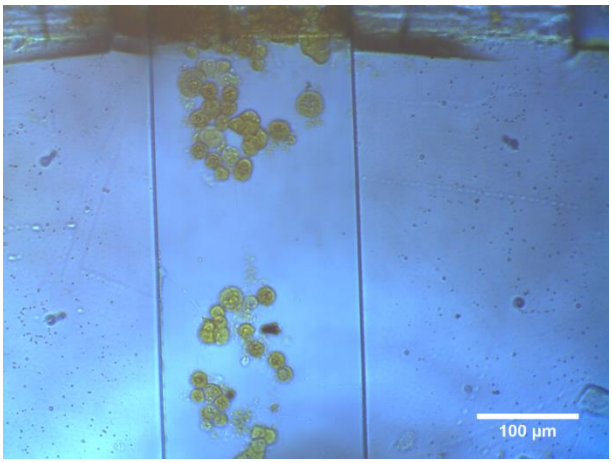

Figure 49 Bright field image of acridine orange (AO) stained MCF-7 cells in epoxy model device IV in the first 0.5 mm to determine highest flow velocity with high cell recovery.

In the first test run, MCF-7 cells were captured in the epoxy model device III with 25% recovery (*Figure 50*). 79% of the captured cells were found in the first 1 mm at 5.6 mm.sec^{-1} (0.134 mL.min^{-1}). Of the cells captured in the first 1 mm (n = 36), the average cell size was 18.8 µm, equal to the cell size determined during cell harvest. This was repeated with other channels with similar results.

The same cell batch was used in a PDMS model device I device at 5.9 mm.sec^{-1} (0.050 mL.min^{-1}) and the average cell size of the captured cells in the first 1 mm (n = 26) was 15.4 µm. This is a significant difference (t-test, $\alpha = 0.05$), so the epoxy model device performed better at capturing the larger cells from the cell batch. No negative control cells were captured in either device. These data confirm the prediction that the decreased channel height increases the likeliness of capturing larger cells. Larger cells experience larger drag force, but in the epoxy device model IV they can bind to the top as well as the bottom antibody-coated surface simultaneously.

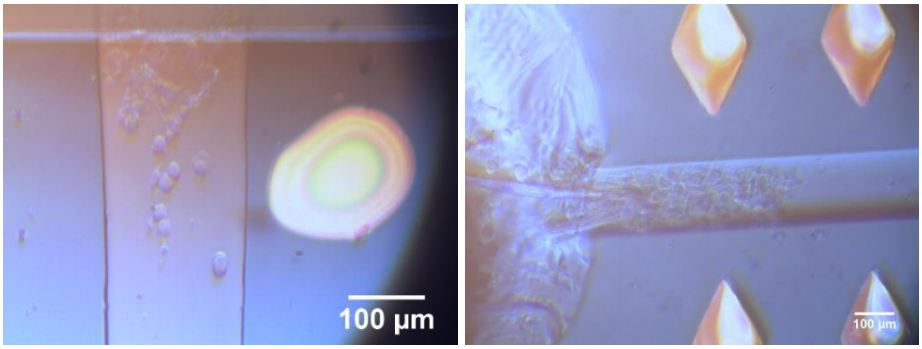

Figure 50 Epoxy model device on the left captured larger cells compared to the PMDS device shown on the right. The void in the epoxy device is air between the epoxy spacer and the top glass slide that could not escape when compressing the top glass slide onto the epoxy spacers during fabrication.

Acridine orange (AO) pre-stained MCF-7 cells were mixed with blood cells to capture the MCF-7 cells while eluting the blood cells. An image (*Figure 51*) was taken during MCF-7 cells enrichment from blood, showing large stagnant cells surrounded by fast-flowing red blood cells. Enrichment from blood was performed several times with promising results. *Figure 52* shows imperfect channels (cells were able to migrate slowly over the spacers) but also that MCF-7 cells could be enriched from whole blood. Red blood cells were not detected after washing with PBS in epoxy model device IV (*Figure 52-A*). Red blood cells were however able to remain attached to the epoxy model device III (*Figure 52-B*), because the top glass slide was not functionalised with PAA chains.

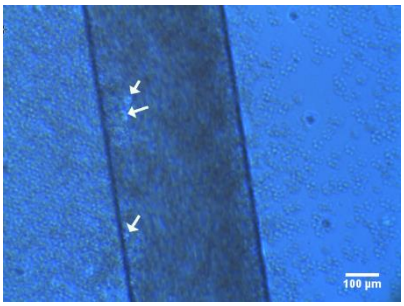

Figure 51 (A) Bright field picture of red blood cells (RBC) flowing fast through the epoxy model device IV, while MCF-7 cells remain attached, easily visible via microscope because the RBCs cannot move below or above the captured cells. The captured MCF-7 cells are indicated with arrows.

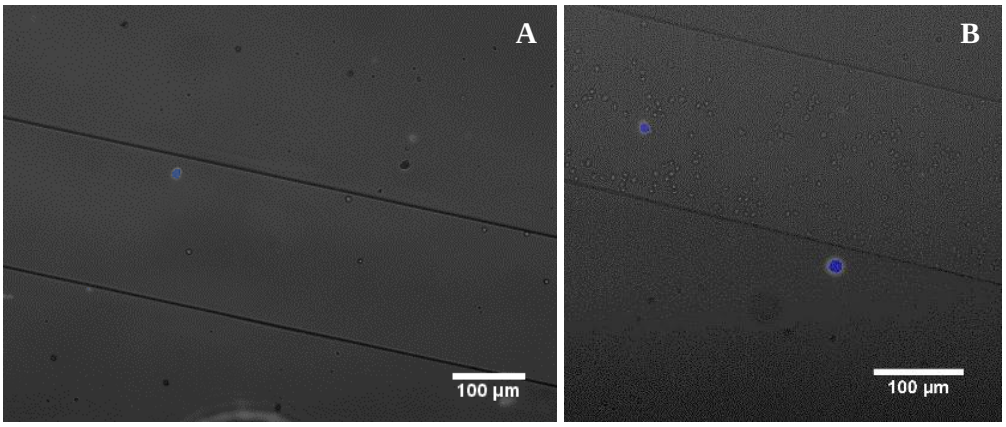

Figure 52 After one washing step with PBS (300 µL), (A) red blood cells were not present in epoxy device model IV, but (B) they were still present in the channel of epoxy model device III, also showing a MCF-7 cells next to the channel.

In the epoxy model device III, the captured cells remained attached at 12.2 mm.sec^{-1} (0.292 mL.min^{-1}) washing step with PBS, although they rolled or moved slightly further into the channel (*Figure 53*). To detach the cells, NaCl solution were effectively used, while increasing the viscosity had negligible effect.

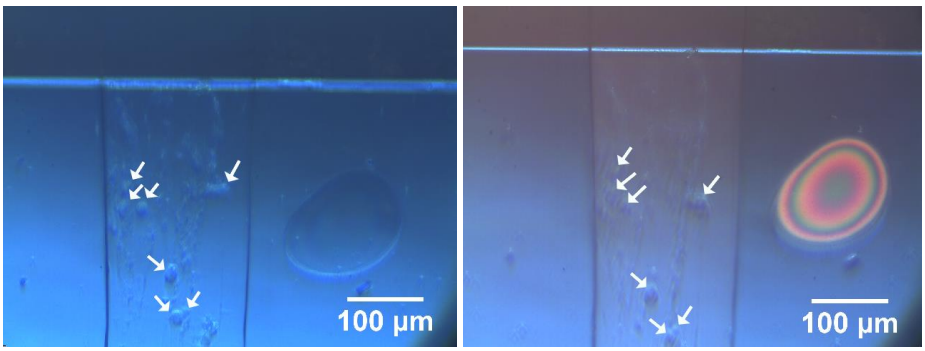

Figure 53 Images taken during washing with PBS at 8.3 mm.sec^{-1} (0.199 mL.min^{-1}, left image) and 12.2 mm.sec^{-1} (0.292 mL.min^{-1}, right image) of epoxy model device. The void appears different in the left image because here only illumination from the top was applied, instead of both top and bottom illumination.

Evaluation of effect of environmental conditions

pH test

The influence of pH on cell detachment was quantified in self-assembled PDMS 11-well plate. It was found that pH 7 and pH 8 induce insignificant detachment of cells (~5% per wash step). pH 9, however, showed an average of 23% cell detachment per wash step, indicating decreased antibody-antigen binding strength. A similar experiment in a channel could be performed to confirm these results for flowing conditions. Cell count results before and washing with a certain pH are shown in *Table 7* and *Figure 54*.

Table 7 Cell counts before and after washing with different pH buffer solutions. Note that unbound cells are washed off with PBS before washing with pH buffers. [A]: no anti-EpCAM coating, so no cell capture expected.

Well	Wash conditions	Cell count before wash	Cell count after wash	Relative change	Average change	SD
A1	pH 7	155	148	-5%		
A2	pH 7	217	209	-4%	-4%	0%
A3	pH 8	246	218	-11%		
A4	pH 8	195	197	1%	-5%	6%
B1	pH 9	175	140	-20%		
B2	pH 9	233	171	-27%	-23%	3%
C1	negative control[A]	9	0	-100%		
C2	negative control[A]	4	0	-100%		

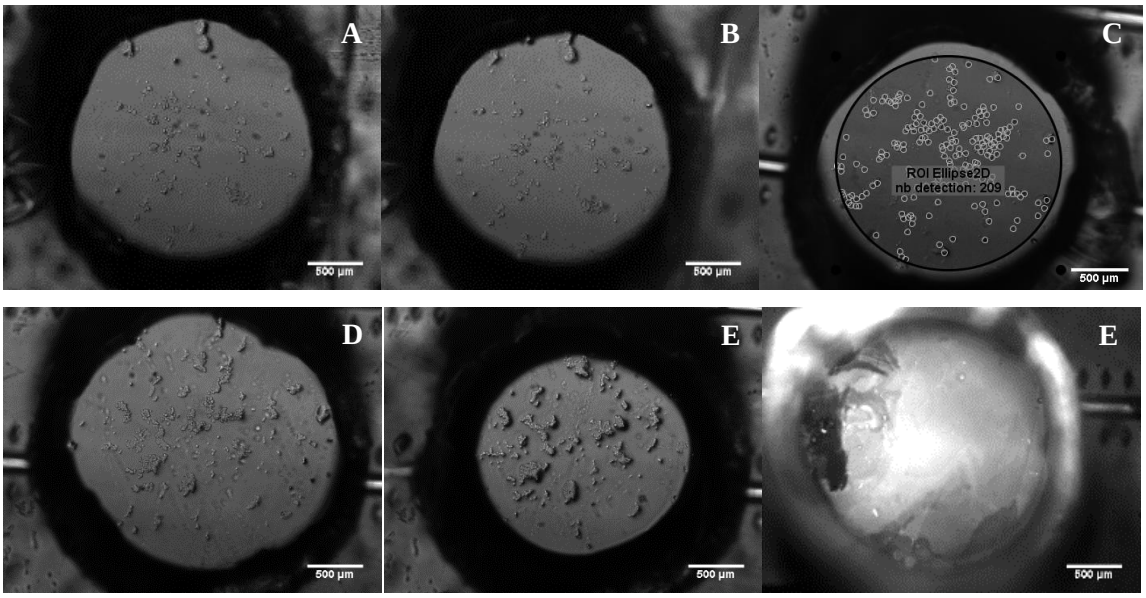

Figure 54 Influence of pH on cell detachment under stationary conditions. (A) and (B) show cell attachment, followed by washing with (D) pH 7 (showing 4.5% detachment), and with (E) pH 9 (showing 20% detachment). (C) Automatic cell enumeration. (F) Validation of antibody functionalisation using IgG-PE to bind immobilised anti-EpCAM.

Viscosity

The viscosities of solutions with different starch content were determined, showing an exponential relation between starch content and viscosity. A starch solution with increased viscosity showed a linear relation (R^2 = 0.995) between flow rate and applied pressure difference, indication the starch solutions in PBS behave as Newtonian fluids (while blood is a shear thinning). Finally, a linear relation was found between viscosity and flow rate (R^2 = 0.964): at the same applied pressure, the flow rate decreases with increasing viscosity. Graphs are in the Appendix, *Figure 58* and *Figure 59*.

After the behaviour of starch solutions was evaluated, cell detachment experiments were performed. No increased cell detachment was observed by increasing the viscosity of the fluid in epoxy devices, without altering the applied pressure gradient. This was in line with the evaluated behaviour of starch solutions. The drag force on captured cells remained constant: increasing the viscosity (drag force increase) automatically decreased the flow velocity (drag force decrease) when the applied pressure gradient was unaltered.

NaCl and demi water

Increased NaCl concentrations were effective at detaching cells from the channel surface. Direct cell rolling and cell detachment were observed when high NaCl concentration solutions (0.92-1.71 M) were added to the reservoirs. Cell shrinkage was not observed. Cell *attachment* under the presence of high NaCl concentration was also investigated. While a 25% cell recovery was achieved with cells in culture medium, a ~10% recovery was observed in five runs with MCF-7 cells in 0.92 M NaCl and ~1% recovery in three runs for MCF-7 cells in 1.71 M NaCl. This data validates that, because NaCl decreases antigen-antibody interaction, cell attachment is based on affinity and not based on size due to the low channel height.

Preliminary results show that detachment of captured cells was also possible by flowing through demineralised water. Demineralised water has, like high molarity NaCl solutions, a different ionic strength compared to culture medium or PBS, which influences the antigen-antibody complex formation. Red blood cells, however, will take up demineralised water until they burst, which causes the release of cell particles that could interfere with the downstream characterisation of captured cell. Therefore, increased ionic strength solutions are up to now the preferred method for intact cell detachment.

Conclusions

This thesis was an explorative feasibility study for continuous enrichment of CTCs from whole blood using microsieves. Model devices were designed, fabricated, and evaluated. Most importantly: nearly all of the captured cells were present in the first 1 mm of the channel in PDMS model I and the epoxy devices. Also, these devices were able to enrich MCF-7 cells from whole blood. These results are proof-of-principle for a microsieve with 1 mm deep pores at continuous operation. It was also proven that cell detachment without cell membrane rupture is possible using high ionic strength solutions as washing fluid. This allows post-capture cell characterisation for assessing the clinical relevance of the CTC enumeration.

The capturing method described in this thesis was selective by the antigen-antibody complex formation: non-coated channels were unable to capture positive control cells, cell attachment in high ionic strength solutions was decreased, cell detachment was increased by a change of pH and ionic strength, and negative control cells were never effectively captured. Previously described affinity-based devices require slow linear flow velocities to capture cells, because the laminar flow pattern makes it unlikely that cells migrate towards the antibody-coated surface. In this thesis, high flow velocities were achieved by employing a channel height equal to the average cell diameter, which forces the cells to interact with the antibody-coated surface. Non-specific binding of blood cells to the antibody coating (100% inner surface coverage in the future microsieve) is unlikely at the proposed flow velocities, so it is expected that the purity of the future microsieve will be high.

Large cells (20 µm) experience larger drag force and are thereby more difficult to capture. By employing a two-sided antibody-coated surface at 20 µm channel height, significantly larger cells were captured compared to a single-sided coated device with 30 µm channel height. Cell recovery was also higher in the channels with low channel height. No entry blockage was observed for the 20 µm channels. These results predict operational success with a future microsieve that will comprise of pores of 20 µm in width.

A 95% cell recovery was achieved in epoxy device model IV at a channel flow rate (sample throughput) of 0.134 mL.min^{-1}. This high sample throughput per channel (25 times higher than previously reported) is due to the low channel aspect ratio (large relative width). This throughput means that a microsieve comprising of 1000 channels with similar geometry would require 37 minutes to perform a full blood screening (5 L), which is very promising for a clinical setting.

Recommendations

On a few aspects, more data are required to draw conclusions. This includes data to validate proposed models for the relation between flow velocity and cell distribution. The current data set implies no relation between flow velocity and cell distribution. A relation between flow velocity and cell recovery was observed, so possibly, if a cell is captured, it will be most likely captured in the first 1 mm of the channel, irrelevant of the flow velocity. Here is was proposed that cell capture is a function of antigen-antibody binding rate, with the binding rate depending on the relative flow velocity of the antigens, the number of antigens the cell presents to the antibody coating at a given moment in time, and cell size. This theory needs validation to conclude the relevance of channel length on cell capture.

The effect of pH on cell detachment was evaluated in self-assembled PDMS 11-well plate. Possibly under flowing conditions, the detachment power of a change of pH might be higher compared to increased ionic strength. Therefore, cell capture and release experiments in microchannels could be performed to determine this.

Cell clumps were often formed between the moment of cell harvest and experiments. Although cell clumps could be present in a clinical sample, they were unwanted during experiments because cell distribution determination becomes more difficult compared to individual cells. Addition of trypsin, vortexing the tube, and pipetting up and down before sample addition to the reservoir were ineffective to separate cells. This trypsin was added to cells in culture medium, which can inactivate the trypsin. Replacing the culture medium with PBS should increase the trypsin efficacy. The addition of EDTA is also recommended to decrease cell-cell adhesion.

It is frequently reported that an increased binding rate and recovery was achieved by employing rough surfaces or microstructures (e.g. micro-posts), with the most striking example being the use of frosted glass slides (Cui et al., 2018). Although such methods allow increased cell capture, they are also more prone to non-specific attachment of blood cells. Biofouling could be a large problem for continuous methods because of clogging and diminished recirculation of blood cells, so smooth channels with only specific cell capture (as was done in this thesis) are recommended to continue with.

Literature References

Adams, A. A., Okagbare, P. I., Feng, J., Hupert, M. L., Patterson, D., Gottert, J., . . . Soper, S. A. (2008). Highly efficient circulating tumor cell isolation from whole blood and label-free enumeration using polymer-based microfluidics with an integrated conductivity sensor. *Journal of the American Chemical Society, 130*(27), 8633-8641. doi:10.1021/ja8015022

Allan, A. L., & Keeney, M. (2010). Circulating tumor cell analysis: technical and statistical considerations for application to the clinic. *J Oncol, 2010*, 426218. doi:10.1155/2010/426218

Andree, K. C., Barradas, A. M., Nguyen, A. T., Mentink, A., Stojanovic, I., Baggerman, J., . . . Terstappen, L. W. (2016). Capture of Tumor Cells on Anti-EpCAM-Functionalized Poly(acrylic acid)-Coated Surfaces. *ACS Appl Mater Interfaces, 8*(23), 14349-14356. doi:10.1021/acsami.6b01241

Baeuerle, P. A., & Gires, O. (2007). EpCAM (CD326) finding its role in cancer. *Br J Cancer, 96*(3), 417-423. doi:10.1038/sj.bjc.6603494

Barteneva, N. S., Ketman, K., Fasler-Kan, E., Potashnikova, D., & Vorobjev, I. A. (2013). Cell sorting in cancer research-Diminishing degree of cell heterogeneity. *Biochimica Et Biophysica Acta-Reviews on Cancer, 1836*(1), 105-122. doi:10.1016/j.bbcan.2013.02.004

Betancourt, T., & Brannon-Peppas, L. (2006). Micro- and nanofabrication methods in nanotechnological medical and pharmaceutical devices. *Int J Nanomedicine, 1*(4), 483-495.

Biosystems, M. S. (2018, 01-03-2018). How does the CELLSEARCH® System work? Retrieved from https://www.cellsearchctc.com/about-cellsearch/how-cellsearch-ctc-test-works

Bockhorn, M., Jain, R. K., & Munn, L. L. (2007). Active versus passive mechanisms in metastasis: do cancer cells crawl into vessels, or are they pushed? *Lancet Oncology, 8*(5), 444-448. doi:Doi 10.1016/S1470-2045(07)70140-7

Bu, P., Chen, K. Y., Xiang, K., Johnson, C., Crown, S. B., Rakhilin, N., . . . Shen, X. (2018). Aldolase B-Mediated Fructose Metabolism Drives Metabolic Reprogramming of Colon Cancer Liver Metastasis. *Cell Metab*. doi:10.1016/j.cmet.2018.04.003

Carter, P. J. (2006). Potent antibody therapeutics by design. *Nat Rev Immunol, 6*(5), 343-357. doi:10.1038/nri1837

Centre, W. M. (2017). Cancer Fact Sheet. Retrieved from http://www.who.int/mediacentre/factsheets/fs297/en/

Chan, A. C., & Carter, P. J. (2010). Therapeutic antibodies for autoimmunity and inflammation. *Nat Rev Immunol, 10*(5), 301-316. doi:10.1038/nri2761

Chang, K. C., & Hammer, D. A. (1999). The forward rate of binding of surface-tethered reactants: effect of relative motion between two surfaces. *Biophysical Journal, 76*(3), 1280-1292. doi:10.1016/S0006-3495(99)77291-7

Coumans, F. A., Ligthart, S. T., Uhr, J. W., & Terstappen, L. W. (2012). Challenges in the enumeration and phenotyping of CTC. *Clin Cancer Res, 18*(20), 5711-5718. doi:10.1158/1078-0432.CCR-12-1585

Coumans, F. A. W., Doggen, C. J. M., Attard, G., de Bono, J. S., & Terstappen, L. W. M. M. (2010). All circulating EpCAM+CK+CD45-objects predict overall survival in castration-resistant prostate cancer. *Annals of Oncology, 21*(9), 1851-1857. doi:10.1093/annonc/mdq030

Cristofanilli, M., Budd, G. T., Ellis, M. J., Stopeck, A., Matera, J., Miller, M. C., . . . Hayes, D. F. (2004). Circulating tumor cells, disease progression, and survival in metastatic breast cancer. *N Engl J Med, 351*(8), 781-791. doi:10.1056/NEJMoa040766

Cui, H., Wang, B., Wang, W., Hao, Y., Liu, C., Song, K., . . . Wang, S. (2018). Frosted Slides Decorated with Silica Nanowires for Detecting Circulating Tumor Cells from Prostate Cancer Patients. *ACS Appl Mater Interfaces, 10*(23), 19545-19553. doi:10.1021/acsami.8b06072

Danila, D. C., Heller, G., Gignac, G. A., Gonzalez-Espinoza, R., Anand, A., Tanaka, E., . . . Scher, H. I. (2007). Circulating tumor cell number and prognosis in progressive castration-resistant prostate cancer. *Clin Cancer Res, 13*(23), 7053-7058. doi:10.1158/1078-0432.CCR-07-1506

Deelstra, F. (2017). *Identification of circulating tumour cell subpopulations.* (Master thesis), University of Twente, Enschede.

Di Carlo, D., Irimia, D., Tompkins, R. G., & Toner, M. (2007). Continuous inertial focusing, ordering, and separation of particles in microchannels. *Proc Natl Acad Sci U S A, 104*(48), 18892-18897. doi:10.1073/pnas.0704958104

Farace, F., Massard, C., Vimond, N., Drusch, F., Jacques, N., Billiot, F., . . . Vielh, P. (2011). A direct comparison of CellSearch and ISET for circulating tumour-cell detection in patients with metastatic carcinomas. *Br J Cancer, 105*(6), 847-853. doi:10.1038/bjc.2011.294

Fargion, S., Carney, D., Mulshine, J., Rosen, S., Bunn, P., Jewett, P., . . . Minna, J. (1986). Heterogeneity of cell surface antigen expression of human small cell lung cancer detected by monoclonal antibodies. *Cancer Res, 46*(5), 2633-2638.

Ferreira, M. M., Ramani, V. C., & Jeffrey, S. S. (2016). Circulating tumor cell technologies. *Mol Oncol, 10*(3), 374-394. doi:10.1016/j.molonc.2016.01.007

Goldsteen, P. A. (2016). *Affinity based capturing of circulating tumour cells inside microfluidic channels.* (MSc), Wageningen University & Research, Enschede.

Haga, T. (1981). Case II swelling of poly (ethylene terephthalate) in organic solvents. *Journal of Applied Polymer Science, 26*(8), 2649-2655.

Harb, W., Fan, A., Tran, T., Danila, D. C., Keys, D., Schwartz, M., & Ionescu-Zanetti, C. (2013). Mutational Analysis of Circulating Tumor Cells Using a Novel Microfluidic Collection Device and qPCR Assay. *Transl Oncol, 6*(5), 528-538.

Henniker-Plasma. (2017). *Plasma Treated PDMS for improved bonding performance of microfluidic devices*. Retrieved from https://plasmatreatment.co.uk/wp-content/uploads/2017/07/Application-Note-Improved-Adhesion-of-PDMS-by-Henniker-Plasma-Treatment.pdf

Hillig, T., Horn, P., Nygaard, A. B., Haugaard, A. S., Nejlund, S., Brandslund, I., & Soletormos, G. (2015). In vitro detection of circulating tumor cells compared by the CytoTrack and CellSearch methods. *Tumour Biol, 36*(6), 4597-4601. doi:10.1007/s13277-015-3105-z

Hong, B., & Zu, Y. (2013). Detecting circulating tumor cells: current challenges and new trends. *Theranostics, 3*(6), 377-394. doi:10.7150/thno.5195

Hong, Y. P., & Zhang, Q. (2016). Phenotype of circulating tumor cell: face-off between epithelial and mesenchymal masks. *Tumor Biology, 37*(5), 5663-5674. doi:10.1007/s13277-016-4796-5

Hosokawa, M., Kenmotsu, H., Koh, Y., Yoshino, T., Yoshikawa, T., Naito, T., . . . Yamamoto, N. (2013). Size-Based Isolation of Circulating Tumor Cells in Lung Cancer Patients Using a Microcavity Array System. *Plos One, 8*(6). doi:ARTN e67466

10.1371/journal.pone.0067466

Huang, H. L., Hsing, H. W., Lai, T. C., Chen, Y. W., Lee, T. R., Chan, H. T., . . . Chan, H. L. (2010). Trypsin-induced proteome alteration during cell subculture in mammalian cells. *J Biomed Sci, 17*, 36. doi:10.1186/1423-0127-17-36

Keum, H., Park, J. K., & Kim, S. (2018). Micro-Lego of 3D SU-8 structures and its application to a re-entrant surface. *Journal of Micro-Bio Robotics*, 1-7.

Konigsberg, R., Obermayr, E., Bises, G., Pfeiler, G., Gneist, M., Wrba, F., . . . Dittrich, C. (2011). Detection of EpCAM positive and negative circulating tumor cells in metastatic breast cancer patients. *Acta Oncol, 50*(5), 700-710. doi:10.3109/0284186X.2010.549151

Langley, R. R., & Fidler, I. J. (2011). The seed and soil hypothesis revisited--the role of tumor-stroma interactions in metastasis to different organs. *International Journal of Cancer, 128*(11), 2527-2535. doi:10.1002/ijc.26031

Liotta, L. A., Kleinerman, J., & Saldel, G. M. (1976). The significance of hematogenous tumor cell clumps in the metastatic process. *Cancer research, 36*(3), 889-894.

Liu, C., & Hu, G. (2017). High-throughput particle manipulation based on hydrodynamic effects in microchannels. *Micromachines, 8*(3), 73.

Lucci, A., Hall, C. S., Lodhi, A. K., Bhattacharyya, A., Anderson, A. E., Xiao, L., . . . Krishnamurthy, S. (2012). Circulating tumour cells in non-metastatic breast cancer: a prospective study. *Lancet Oncology, 13*(7), 688-695. doi:10.1016/S1470-2045(12)70209-7

Macdonald, J., Henri, J., Roy, K., Hays, E., Bauer, M., Veedu, R. N., . . . Shigdar, S. (2018). EpCAM Immunotherapy versus Specific Targeted Delivery of Drugs. *Cancers (Basel), 10*(1). doi:10.3390/cancers10010019

Martel, J. M., & Toner, M. (2014). Inertial focusing in microfluidics. *Annu Rev Biomed Eng, 16*, 371-396. doi:10.1146/annurev-bioeng-121813-120704

Moran, S., Martinez-Cardus, A., Sayols, S., Musulen, E., Balana, C., Estival-Gonzalez, A., . . . Esteller, M. (2016). Epigenetic profiling to classify cancer of unknown primary: a multicentre, retrospective analysis. *Lancet Oncology, 17*(10), 1386-1395. doi:10.1016/S1470-2045(16)30297-2

Moreno, J. G., Miller, M. C., Gross, S., Allard, W. J., Gomella, L. G., & Terstappen, L. W. (2005). Circulating tumor cells predict survival in patients with metastatic prostate cancer. *Urology, 65*(4), 713-718. doi:10.1016/j.urology.2004.11.006

Muschel, R. J. (2011). Metastasis. In M. Schwab (Ed.), *Encyclopedia of Cancer* (pp. 2260-2261). Berlin, Heidelberg: Springer Berlin Heidelberg.

Mutter, T. C., Ruth, C. A., & Dart, A. B. (2013). Hydroxyethyl starch (HES) versus other fluid therapies: effects on kidney function. *Cochrane Database Syst Rev*(7), CD007594. doi:10.1002/14651858.CD007594.pub3

Nagrath, S., Sequist, L. V., Maheswaran, S., Bell, D. W., Irimia, D., Ulkus, L., . . . Toner, M. (2007). Isolation of rare circulating tumour cells in cancer patients by microchip technology. *Nature, 450*(7173), 1235-1239. doi:10.1038/nature06385

Ng, E., Hoshino, K., & Zhang, X. J. (2013). Microfluidic immunodetection of cancer cells via site-specific microcontact printing of antibodies on nanoporous surface. *Methods, 63*(3), 266-275. doi:10.1016/j.ymeth.2013.07.043

Ng, S. Y., Reboud, J., Wang, K. Y. P., Tang, K. C., Zhang, L., Wong, P., . . . Chen, Y. (2010). Label-free impedance detection of low levels of circulating endothelial progenitor cells for point-of-care diagnosis. *Biosensors & Bioelectronics, 25*(5), 1095-1101. doi:10.1016/j.bios.2009.09.031

Ni, J., Cozzi, P. J., Duan, W., Shigdar, S., Graham, P. H., John, K. H., & Li, Y. (2012). Role of the EpCAM (CD326) in prostate cancer metastasis and progression. *Cancer Metastasis Rev, 31*(3-4), 779-791. doi:10.1007/s10555-012-9389-1

Nima, Z. A., Mahmood, M., Xu, Y., Mustafa, T., Watanabe, F., Nedosekin, D. A., . . . Biris, A. S. (2014). Circulating tumor cell identification by functionalized silver-gold nanorods with multicolor, super-enhanced SERS and photothermal resonances. *Sci Rep, 4*, 4752. doi:10.1038/srep04752

Pailler, E., Oulhen, M., Billiot, F., Galland, A., Auger, N., Faugeroux, V., . . . Farace, F. (2016). Method for semi-automated microscopy of filtration-enriched circulating tumor cells. *Bmc Cancer, 16*. doi:ARTN 477

10.1186/s12885-016-2461-4

Pantel, K., Deneve, E., Nocca, D., Coffy, A., Vendrell, J. P., Maudelonde, T., . . . Alix-Panabieres, C. (2012). Circulating epithelial cells in patients with benign colon diseases. *Clinical Chemistry, 58*(5), 936-940. doi:10.1373/clinchem.2011.175570

Perry, G., Thomy, V., Das, M. R., Coffinier, Y., & Boukherroub, R. (2012). Inhibiting protein biofouling using graphene oxide in droplet-based microfluidic microsystems. *Lab on a Chip, 12*(9), 1601-1604. doi:10.1039/c2lc21279j

Plaks, V., Koopman, C. D., & Werb, Z. (2013). Circulating tumor cells. *Science, 341*(6151), 1186-1188. doi:10.1126/science.1235226

Qian, C.-N., & Teh, B. T. (2011). "Seed and Soil" Theory of Metastasis. In M. Schwab (Ed.), *Encyclopedia of Cancer* (pp. 3354-3355). Berlin, Heidelberg: Springer Berlin Heidelberg.

Radisic, M., Iyer, R. K., & Murthy, S. K. (2006). Micro- and nanotechnology in cell separation. *International Journal of Nanomedicine, 1*(1), 3-14. doi:DOI 10.2147/nano.2006.1.1.3

Raghavan, M., Bonagura, V. R., Morrison, S. L., & Bjorkman, P. J. (1995). Analysis of the pH dependence of the neonatal Fc receptor/immunoglobulin G interaction using antibody and receptor variants. *Biochemistry, 34*(45), 14649-14657.

Riethdorf, S., Fritsche, H., Muller, V., Rau, T., Schindlbeck, C., Rack, B., . . . Pantel, K. (2007). Detection of circulating tumor cells in peripheral blood of patients with metastatic breast cancer: a validation study of the CellSearch system. *Clin Cancer Res, 13*(3), 920-928. doi:10.1158/1078-0432.CCR-06-1695

Rodewald, R. (1976). pH-dependent binding of immunoglobulins to intestinal cells of the neonatal rat. *J Cell Biol, 71*(2), 666-669.

Ross, A. A., Cooper, B. W., Lazarus, H. M., Mackay, W., Moss, T. J., Ciobanu, N., . . . et al. (1993). Detection and viability of tumor cells in peripheral blood stem cell collections from breast cancer patients using immunocytochemical and clonogenic assay techniques. *Blood, 82*(9), 2605-2610.

Ruf, P., Gires, O., Jager, M., Fellinger, K., Atz, J., & Lindhofer, H. (2007). Characterisation of the new EpCAM-specific antibody HO-3: implications for trifunctional antibody immunotherapy of cancer. *Br J Cancer, 97*(3), 315-321. doi:10.1038/sj.bjc.6603881

Saucedo-Zeni, N., Mewes, S., Niestroj, R., Gasiorowski, L., Murawa, D., Nowaczyk, P., . . . Lucke, K. (2012). A novel method for the in vivo isolation of circulating tumor cells from peripheral blood of cancer patients using a functionalized and structured medical wire. *Int J Oncol, 41*(4), 1241-1250. doi:10.3892/ijo.2012.1557

Schwab, M. (2011). Circulating Tumor Cells. In M. Schwab (Ed.), *Encyclopedia of Cancer* (pp. 865-868). Berlin, Heidelberg: Springer Berlin Heidelberg.

Singer, S. J. (1972). A fluid lipid-globular protein mosaic model of membrane structure. *Ann N Y Acad Sci, 195*, 16-23.

Sleijfer, S., Gratama, J. W., Sieuwerts, A. M., Kraan, J., Martens, J. W. M., & Foekens, J. A. (2007). Circulating tumour cell detection on its way to routine diagnostic implementation? *European Journal of Cancer, 43*(18), 2645-2650. doi:10.1016/j.ejca.2007.09.016

StatLine, C. (2017, 27-12-2017). Overledenen; belangrijke doodsoorzaken (korte lijst), leeftijd, geslacht. Retrieved from https://opendata.cbs.nl/statline/#/CBS/nl/dataset/7052_95/table?dl=541E

StatLine, C. (2018, 29-12-2017). Health, lifestyle, health care use and supply, causes of death; from 1900. Retrieved from https://opendata.cbs.nl/statline/#/CBS/en/dataset/37852eng/table?ts=1527499761478

Sterzynska, K., Kempisty, B., Zawierucha, P., & Zabel, M. (2012). Analysis of the specificity and selectivity of anti-EpCAM antibodies in breast cancer cell lines. *Folia Histochem Cytobiol, 50*(4), 534-541. doi:10.5603/17845

Stoecklein, N. H., Fischer, J. C., Niederacher, D., & Terstappen, L. W. (2016). Challenges for CTC-based liquid biopsies: low CTC frequency and diagnostic leukapheresis as a potential solution. *Expert Rev Mol Diagn, 16*(2), 147-164. doi:10.1586/14737159.2016.1123095

Strati, A., Kasimir-Bauer, S., Markou, A., Parisi, C., & Lianidou, E. S. (2013). Comparison of three molecular assays for the detection and molecular characterization of circulating tumor cells in breast cancer. *Breast Cancer Res, 15*(2), R20. doi:10.1186/bcr3395

Swennenhuis, J. F., Reumers, J., Thys, K., Aerssens, J., & Terstappen, L. W. (2013). Efficiency of whole genome amplification of single circulating tumor cells enriched by CellSearch and sorted by FACS. *Genome Med, 5*(11), 106. doi:10.1186/gm510

Szmulewitz, R., Taylor, J., & Rinker-Schaffer, C. (2011). Metastatic Colonization. In M. Schwab (Ed.), *Encyclopedia of Cancer* (pp. 2271-2273). Berlin, Heidelberg: Springer Berlin Heidelberg.

Takeichi, M. (1988). The cadherins: cell-cell adhesion molecules controlling animal morphogenesis. *Development, 102*(4), 639-655.

Tan, S. H., Nguyen, N. T., Chua, Y. C., & Kang, T. G. (2010). Oxygen plasma treatment for reducing hydrophobicity of a sealed polydimethylsiloxane microchannel. *Biomicrofluidics, 4*(3), 32204. doi:10.1063/1.3466882

Theil, G., Fischer, K., Weber, E., Medek, R., Hoda, R., Lucke, K., & Fornara, P. (2016). The Use of a New CellCollector to Isolate Circulating Tumor Cells from the Blood of Patients with Different Stages of Prostate Cancer and Clinical Outcomes - A Proof-of-Concept Study. *Plos One, 11*(8), e0158354. doi:10.1371/journal.pone.0158354

Vona, G., Sabile, A., Louha, M., Sitruk, V., Romana, S., Schutze, K., . . . Paterlini-Brechot, P. (2000). Isolation by size of epithelial tumor cells - A new method for the immunomorphological and molecular characterization of circulating tumor cells. *American Journal of Pathology, 156*(1), 57-63. doi:Doi 10.1016/S0002-9440(10)64706-2

Wang, L., Balasubramanian, P., Chen, A. P., Kummar, S., Evrard, Y. A., & Kinders, R. J. (2016). Promise and limits of the CellSearch platform for evaluating pharmacodynamics in circulating tumor cells. *Semin Oncol, 43*(4), 464-475. doi:10.1053/j.seminoncol.2016.06.004

Yao, X., Labelle, M., Lamb, C. R., Dugan, J. M., Williamson, C. A., Spencer, D. R., . . . Wittrup, K. D. (2013). Determination of 35 cell surface antigen levels in malignant pleural effusions identifies CD24 as a marker of disseminated tumor cells. *International Journal of Cancer, 133*(12), 2925-2933. doi:10.1002/ijc.28312

Yusa, A., Toneri, M., Masuda, T., Ito, S., Yamamoto, S., Okochi, M., . . . Nakanishi, H. (2014). Development of a New Rapid Isolation Device for Circulating Tumor Cells (CTCs) Using 3D Palladium Filter and Its Application for Genetic Analysis. *Plos One, 9*(2). doi:ARTN e88821

10.1371/journal.pone.0088821

Zhang, J., Yan, S., Yuan, D., Alici, G., Nguyen, N. T., Ebrahimi Warkiani, M., & Li, W. (2016). Fundamentals and applications of inertial microfluidics: a review. *Lab on a Chip, 16*(1), 10-34. doi:10.1039/c5lc01159k

Appendix

Tube length and orientation

It was found that tubing filled with air can be positioned in any orientation at any length without altering the fluid flow rate, presumably because the pressure loss by elevation and by the pressure loss by friction with the tubing are small. The hydrostatic pressure drop by elevation is not negligible and was even used to create small flow rates in the channel. A water height difference of 1 cm creates a 1 mBar pressure gradient:

$$\Delta p = \rho \cdot g \cdot h$$

In this research, we worked with 5 mBar pressure gradients using the pump, which means that a small incline in the tubing results in significant pressure inaccuracies.

Cell settling

Binding or settling of cells in the region in front of the entrance (e.g. the reservoir) was statistically not a problem in this research, as these cells or vesicles can be ignored in the measurements. The number of cells settled was so high (the full surface of the reservoir could be filled with cells), that there were not many cells left to enter the channel. At very low flow rates, the number of cells that entered the channel was very low due to sedimentation and cell attachment in the reservoir. It might be a problem, because the cells that are least likely to bind with the EpCAM layer, were the most likely to enter the channel.

Other device fabrication methods and recommendations

The current device design was made after several other designs were evaluated, which are discussed in this section.

Glass etching using KOH and NaOH: the PDMS chip used as a 'mould' for glass etching was damaged on a microstructure level by both bases. Everywhere the fluid found its way between the PDMS chip and the glass slide, the bond between the PDMS and the glass broke. Binding the chip with flexible plastic tubing was also not successful because the KOH concentration was too low for effective glass etching. Increasing the concentration led to microstructure destruction on the PDMS surface.

The interaction of PDMS with KOH and NaOH was quantified by measuring the weight decrease of PDMS chips before and after 1 hour exposure at ~80ºC. Of all ten chips (exposed and measured two times), the weight decrease was only 0.1%. On a microstructure level, however, 40% KOH and 40% NaOH were quite destructive. Data shown in *Appendix - Results of interaction of PDMS with KOH and NaOH quantification*.

Glass etching using HF: HF was used to etch glass with vinyl glue as mask. A 5-10% HF solution stopped the vinyl glue adhesive power to the glass after 60 minute treatment. Because the vinyl glue detached, precise channels could not be created. Using different glass (e.g. soda lime glass) instead of Borofloat would increase the etch rate, thereby requiring less reaction time. Temporarily attach a top glass slide to decrease the likeliness of glue detachment.

Solution to initial mould problems: PDMS replication: PDMS structures were treated for 10-25 minutes with chloro-trimethyl silane vapour. Without curing step this method was ineffective for PDMS coating for microstructures.

PDMS replication 2: PDMS structures were submerged for 2 minute in detergent/ethanol: five squirts mild liquid soap detergent was mixed with 45 mL ethanol for a cloudy suspension. A 24 hour exposure damaged the PDMS microstructures, which was observed under the microscope after cleaning the chip with ethanol and adhesive tape. *Figure 55* shows the result on the microstructures of PDMS.

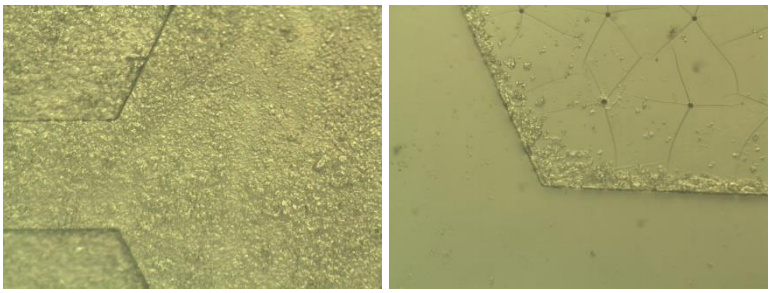

Figure 55 Microstructure destruction of PDMS by detergent in ethanol.

Entry and exit from PET: Innofil PET structures were 3D-printed and melted or glued on the glass slide. Several melting methods were evaluated. For example, dipping the print in the fluid and directly placing it onto the glass also melts the entry arch and e.g. the epoxy or vinyl glue spacers. Dipping and washing in water, dipping and placing it on dry or wet paper, melting with humidified paper were all methods that were subordinate to dipping in the fluid and blowing the residual droplets away with pressurised N_2 gas.

The entry print required an arch to connect the reservoir to the channel. Melting an arch using a hot needle and cutting the arch by hand were effective but not reproducible methods. The Ultimaker 2 was able to make the basis of the arch, which was best finished by hand using a scalpel.

Table 8 Results of PET melting tests using different chemicals.

Chemical	PET melting power		Ability to be used
100% dichloromethane (DCM)	+++	Dip in fluid and blow away residual droplets.	+
100% chloroform	++	Dip in fluid and blow away residual droplets.	+
100% toluene	+/-	10 second submersion.	--
98% acetone	+	5 second submersion.	-

Entry and exit from PDMS: From a simple PDMS block, an entry can be created by puncturing the block with a 5 mm punch and creating a small arch with the 1 mm punch. In theory this could bind tightly to glass, but the cutting lines were not straight enough for perfect annealing of the PDMS with the top glass slide. Glue cannot be used on PDMS to seal the gaps.

Evaluation of different glues: Bison Universal, Cre-Action all-glue, PDMS, two types of quick-curing epoxy resin, nail polish, and fluid silicone rubber were evaluated based on their ability to creep into narrow spaces using several tests. The results are shown in Table 9.

Table 9 Results of glue evaluation tests.

Glue	Curing	Capillary action	Curing time	Control over the fabrication process	Ability to seal entry/exit prints
Bison Universal	No air bubbles, transparent	+	--	+/-	-
Cre-Ation universal	Many air bubbles, white gauze	--	-	+/-	-
PDMS	No air bubbles, transparent	++	+	-	+
Epoxy resin 2 hour curing	No air bubbles, yellow-ish	-	+/-	+	+
Epoxy resin 5 min curing	No air bubbles, yellow-ish	-	+	+	+
Nail gel polish	Many air bubbles, pink-ish	--	--	+	-
Silicone rubber	Gauze, transparent	++	--	--	-
BioniQ UV	No air bubbles, transparent	+	++	++	+
100% chloroform	NA	NA	NA	+/-	++

Cura 2.3.0 settings

Table 10 Cura 2.3.0 settings

Parameter	**Value**
Layer height (*Initial layer height*)	0.06 (*0.1*)
Line width	0.4
Wall Thickness (*Bottom Thickness*)	0.8 (*0.1*)
Top/Bottom Pattern	Lines
Infil Density	100%
Infill Layer Thickness	0.06
Print Speed	30 $mm.s^{-1}$
Build Plate Adhesion Type, Brim Width	Brim (*8.0 mm*)

Results of conductivity measurements of different NaCl solutions

Table 11 Conductivity of several solutions after 3 minutes of measuring per sample.

Solution	**Molarity**	**Ohm (2000 k Ohm setting)**	**Error estimate**
Tap water	0.002	1090	10
Tap water		1209	20
Tap water		1221	20
Tap water		1200	20
1/10x PBS	0.015	1350	10
1/10x PBS		1390	20
1/10x PBS		1044	10
1/3x PBS	0.050	1040	20
1/3x PBS		1170	10
1/3x PBS		1026	10
1xPBS	0.150	910	20
1xPBS		880	10
1xPBS		780	20
1xPBS		1061	20
1xPBS 10 mL + 0.5 gr NaCl	1.07	739	5
1xPBS 10 mL + 0.5 gr NaCl		760	20
15 mL DW + 0.3 gr NaCl	0.34	233	5
15 mL DW + 1.0 gr NaCl	1.14	188	5

Results of interaction of PDMS with KOH and NaOH quantification

Table 12 Quantification of PDMS interaction with etching solutions.

Beaker number	Weight before (gram)	Weight after 1 h drying	Weight after 24 h drying	Difference	Relative decrease
1 - 50% KOH	0.9841	0.9827	0.9819	-0.0022	0%
1 - 50% KOH	0.8373	0.8366	0.8359	-0.0014	0%
1 - 50% KOH	0.7687	0.7673	0.7664	-0.0023	0%
2 - 50% KOH	0.8059	0.8052	0.8044	-0.0015	0%
2 - 50% KOH	0.7149	0.7147	0.7135	-0.0014	0%
3 - 20% NaOH	0.9109	0.9110	0.9099	-0.001	0%
3 - 20% NaOH	0.7916	0.7922	0.7906	-0.001	0%
3 - 20% NaOH	0.7062	0.7065	0.7052	-0.001	0%
4 - 20% NaOH	0.7963	0.7968	0.7953	-0.001	0%
4 - 20% NaOH	0.8837	0.8848	0.8831	-0.0006	0%

Filling of the PDMS mould for epoxy model I and II

Figure 56 Epoxy resin is added on top of the PDMS structure. The epoxy resin fills the mould through the punctured holes via capillary action. The arrow indicates the epoxy interface; the mould is filled half-way in this picture. Filling takes ~20 minutes.

Newton rings visible after placing a glass slide on top of the epoxy spacers

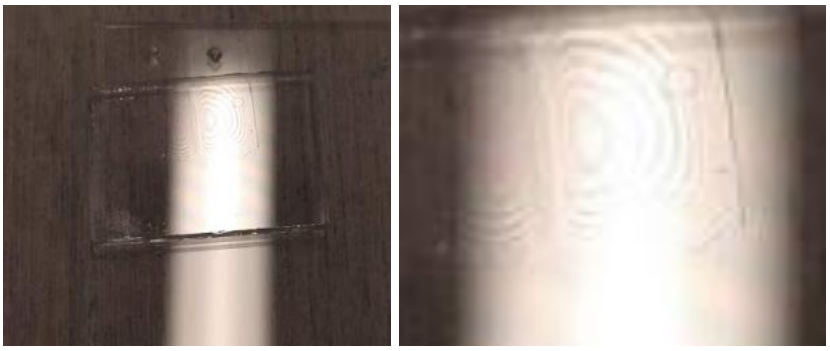

Figure 57 Bottom glass slide with epoxy spacers and a small top glass slide on top of the spacer created lines. The lines are Newton rings caused by light interference by height variation. Interpret it as an elevation map with each line corresponding to a certain height and the circle in the middle as the lowest point.

Behaviour in the channel of fluids with different viscosities

A flow rate decrease of 15% was observed with 0.67% g/v starch solution in PBS compared to pure PBS. This effect relative to PBS became gradually smaller with increasing flow rate. Because low flow rates were used in this research, using starch solution (to decrease the flow rate even more) was considered an option. However, the starch solution of 0.67% g/v was unpredictable below 18 mBar (~0.0023 mL.min^{-1}), as the flow could not always be initiated. On top of this, increasing the starch concentration to more than 2% g/v requires 380% pressure difference increase to flow at the same velocity as pure PBS.

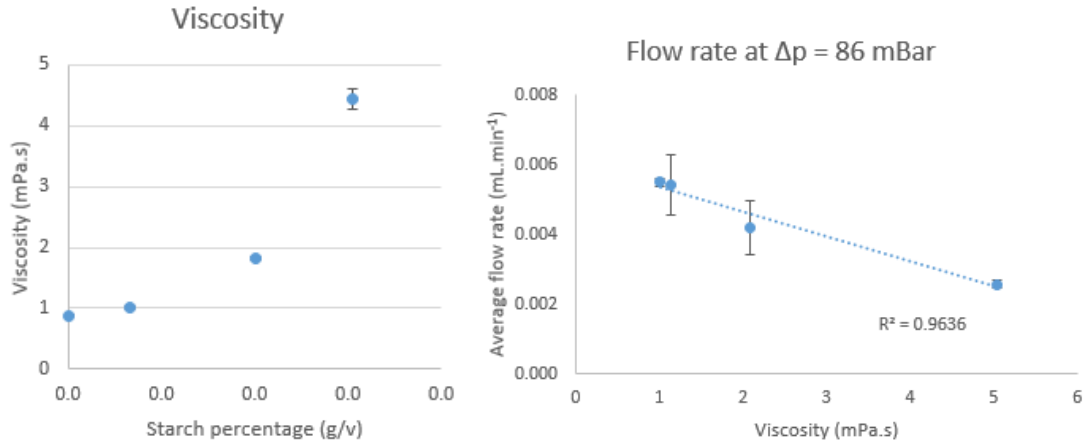

Figure 58 Viscosity in mPa.s as a function of starch percentage in gram per mL PBS. The flow velocity decreases with increasing viscosity when applying a constant pressure gradient.

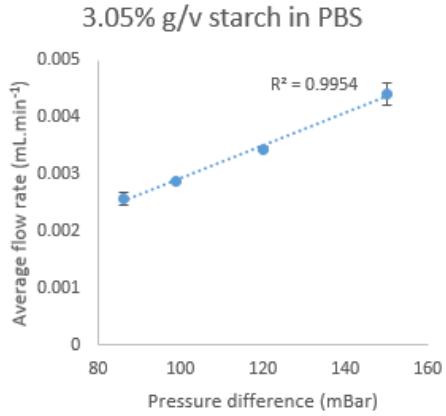

Figure 59 Starch solution behaves like a Newtonian fluid.